Autonomous Vertical Recovery of Fixed Wing Unmanned Aerial Vehicles

by

Trevor R. Smouter

A thesis
presented to the University of Waterloo
in fulfillment of the
thesis requirement for the degree of
Master of Applied Science
in
Electrical and Computer Engineering

Waterloo, Ontario, Canada, 2013

AUTHOR'S DECLARATION

I hereby declare that I am the sole author of this thesis. This is a true copy of the thesis, including any required final revisions, as accepted by my examiners.

I understand that my thesis may be made electronically available to the public.

Abstract

As unmanned aerial vehicles (UAVs) prevail in commercial and first responder applications, the need for safer and more consistent recovery methods is growing. Standard aircraft landing manoeuvres are only possible with a suitable runway which is often unavailable outside of military applications. Alternative recovery approaches can be either contained within the aircraft, ie. parachute or be setup on the ground ie. net landing. By integrating the recovery system into the vehicle, the flight preparation can be streamlined due to the fact that setting up recovering devices is no longer required. The goal of this thesis is to investigate the application of an autonomous vertical landing capability for fixed wing UAVs using articulated motors to enter vertical flight. Using an experimental UAV design, the dynamics of the problem were investigated using recorded flight data. Implementing a decoupled control approach, the aircraft was stabilized to maintain a horizontal hover. Through the characterized plant model that defines the vertical descent behaviour, a control topology was developed and tested in simulation using an optimal control approach. The developed controller was tested on the experimental UAV to verify the vertical landing performance. It was determined that this approach was well suited to autonomous vertical recovery of a fixed wing UAV. In employing this approach to UAV recovery, operators can easily operate in theatres where space for conventional landing does not exist.

Acknowledgements

I would like to sincerely thank my supervisor, Professor David Wang, who provided guidance throughout my research activities, mentored me in the ways of grad school and generally taught me to calm down a little. I would also like to thank my readers, Professor Glenn Heppler and Professor Daniel Davison for their time and counsel.

I would like to thank my friends Steve Buchanan and Ryan Tuner for the assistance they provided me during my research experiments.

Finally, I must thank my wife Sarah, without her none of this would have been possible.

Dedication

This thesis is dedicated to my family:

First and foremost it is dedicated to my wife Sarah and our children Jacob and James. Without their steadfast love, support, encouragement and understanding my education would not have been possible.

To my mother, Annette, who cultivated my intelligence, inspired me to always reach higher and who navigated my early education with a steady hand.

Also to my father Robert, whose technical abilities, strong work ethic and discipline have set the example and made me the engineer I am today.

Table of Contents

List of Figures

List of Tables

Chapter 1
Introduction

For over the past 100 years of heavier-then-air manned flight, there has been a common aphorism spoken among aviators – *it is better to be on the ground wishing you were in the air then to be in the air wishing you were on the ground*. While it is a cautious statement that "take-off is optional but landing is mandatory", it does not belie the fact that crashing is also in certain terms a landing. Difficulties are compounded when the landing of aircrafts do not have the benefit of a prepared airfield as is commonplace in UAV (unmanned aerial vehicle) missions.

The current growth in UAV system technologies and their emerging civil and commercial applications [1] has brought about many new applications where modern control theory is used as a tool to increase the performance and capabilities of the vehicles in this rapidly growing field. Applications for alternative recovery methods are as varied as the uses for small UAVs. Typical commercial applications for small UAVs routinely include mapping, surveying and aerial photography [2]. Accuas Inc., a Canadian company, often flies missions for clients to create 3D maps of quarries, mines and waste management sites necessary for both monitoring these sites as well as for future planning [2]. Also, Unmanned Systems Canada provides competitions for teams using UAVs for wildfire management in addition to search and rescue operations [3]. Operating out of these numerous areas provide challenges for recovery since the areas are most often unpredictable, uneven and/or built up with brush. Conventional landing requires long gentle glide slopes to keep low airspeed and low flight path angles. The old aviator's adage that *the probability of survival is inversely related to the angle of arrival* definitely applies.

Over the past decade, new electric propulsion system technologies for aircraft have reshaped model aviation and concurrently changed the landscape of small UAV systems and applications. Electric propulsion has led to the proliferation of a family of vertical take-off and landing (VTOL) UAVs known as multi rotor aircraft, which rely on the high bandwidth response unique to electric propulsion in order to achieve stability. While these aircraft benefit from their simplicity due to very few moving parts as compared to other VTOL aircraft, ie. helicopters, they lack the efficiency and range required for many UAV applications. The most common UAVs for military and commercial applications remain the fixed wing aircraft due to their much higher efficiency and subsequently longer range and longer duration missions. Small fixed wing UAVs also benefit from the new electric propulsion technologies. The electric motor is nearly vibration free compared with the

alternative combustion engines, leading to better payload capabilities. For instance, electric propulsion allows optical systems that are sensitive to vibration. Other benefits include the ability to stop and start the motor in flight, cleaner operation and a much lower noise pollution. These features foster operations which are more flexible, especially for commercial operators where missions are most likely to be conducted in noise sensitive areas.

The rise of commercial applications for small UAVs and the growing acceptance of these activities by their respective governing agencies have allowed UAV operations to push into areas where aviation infrastructure, ie. runways, are often unavailable. Currently, the largest impediments to these operations are UAV recovery which ultimately governs the mission success. If the UAV is damaged during the recovery process, it most often means that operations must be temporarily suspended until the necessary repairs can be completed. Much of the time take-off is not a problem as it can be easily accomplished by hand-launch, slingshot or pneumatic catapult [4] depending on the size of the UAV. Many mobile commercial UAVs are of a hand launch size. If an adequate prepared strip is unavailable for standard landing recovery, as is often the case for commercial operators, then common alternatives include net-landing or parachute recovery. Both of these options remain high risk. Net landing risks occur where the pilot is required to manually fly the UAV into a net which is of similar construction to a volley ball net. Clearly, this is a difficult task to execute in that it requires a highly skilled pilot for the mission operation as well as excluding the option of autonomous landing. Even if the net is hit squarely, there is a large possibility that the UAV will either flip forward over the net or bounce back out, often landing on the tail and causing damage that suspends the mission flights. While other recovery methods exist for these areas, such as trailered net landings or Institu's Scan Eagle recovery known as the skyhook (Figure 1), they require large trailers and are more suited to their military applications.

Figure 1: Insitu's ScanEagle being caught by the SkyHook

The aforementioned technology is out of reach for commercial operators or first responders. The parachute landing also has many draw backs since successful deployment is critical where a tangled chute often leads to the total loss of the aircraft. Should the chute successfully deploy, control of the UAV landing is lost, making operations near wooded areas or above open water extremely risky. Further, even with a moderate wind speed, the UAV will be landing with a similar ground speed at an unknown attitude which is very risky.

An alternative approach is a fixed wing aircraft capable of a vertical descent. This approach would allow easy operations in typical mission areas and provide the ability to operate in areas where none of the aforementioned technologies can operate such as densely populated urban areas. One of the main advantages of this type of technology is the ability to rapidly deploy the UAV without the worry of recovery preparation. This is a crucial asset to commercial operators but significantly more desirable for first responder applications where operation flexibility and quick deployment can make the difference for a successful mission.

The subject of this thesis is applied research towards the goal of autonomous, controlled and low risk small UAV recovery. Building on the current state of art in typical small fixed wing UAVs using modern electric propulsion systems, a novel approach at UAV recovery is explored that provides controlled autonomous vertical descent and landing. The proposed approach for successful execution

of this recovery system is to design a fixed wing UAV with wing mounted main motors in a standard twin configuration called the Lux Aether shown in Figure 2 and Figure 3.

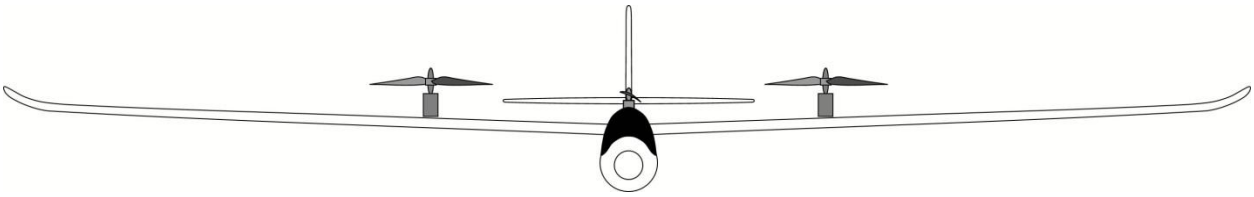

Figure 2: Front view of the Lux with motors in vertical position

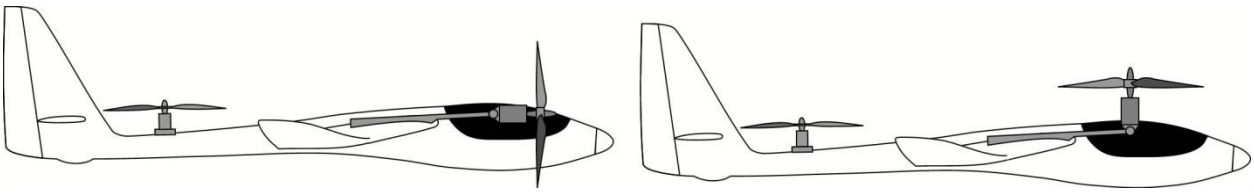

Figure 3: The Lux shown with motors in the forward flight and vertical landing positions

This design differentiates from the conventional twin configuration in that the main motors are articulated to enable rotating the motors from a standard forward facing position to an upwards facing direction, allowing a range of motion where thrust vectoring occurs in both positions. The design also incorporates a small vertical motor in the tail section of the fuselage providing pitch stability in vertical descent mode. Leveraging the high bandwidth control of the electric propulsion system, the vertical descent is controlled in a manner similar to multi-rotor aircraft. To ensure that the UAV is viable for commercial use, it is prudent to use the main motors for both forward flight as well as descent in order to save weight, as opposed to simply adding extra motors to do the vertical landing. Major challenges in this research were designing the vertical landing capabilities necessary when working with an aircraft that is optimized for forward flight. Aligning the center of gravity with the wing becomes critical to maintaining forward flight controllability. Likewise, the approach success rests on lifting the majority of the aircraft's weight using the main motors to ensure there is limited propulsion redundancy in the system. Further, the control system is unique from a typical multi-rotor since the system is highly asymmetrical due to weight and propulsion distribution and must therefore contend with the unique challenges of controlling a large aerodynamic system at airspeeds required to counteract wind to maintaining zero ground speed for landing.

This thesis discusses the topic background including prior art. The thesis then presents the unique experiment designed to conduct the thesis research. Analysis of the plant dynamics is undertaken to formulate a control system topology in addition to identifying the governing system model. In applying this understanding while considering sensor limitations, a controller is developed and tested within simulation. The success of the design is evaluated by testing the controller experimentally where results are compared to those of the simulation. In closing, a conclusion with future research is provided.

Chapter 2
Background

Autonomous recovery of a fixed wing UAV using vertical flight hails from research into vertical take-off and landing (VTOL) aircraft, although this application is focused only on the landing portion of the technology. The first recorded evidence of humans contemplating heavier than air VTOLs similar to helicopters we know today was Leonardo da Vinci's helicopter drawings from 1493 [5]. Approximately 450 years later, early rotary wing helicopter prototypes would take to the air in leaps and bounds. While the roots of fixed wing aircraft technologies can be easily traced to its respective inventors, the helicopter has a more muddied history with many inventors [6]. The modern helicopter design we know today is largely attributed to Igor Sikorsky and consisted of a main lifting rotor with cyclic controls for pitch and roll control with a sideward thrusting tail rotor for anti-torque and yaw control [6]. With production versions appearing in 1941, applications for the reliable VTOL aircraft were military focused. The ability of the helicopter to take off and land without a prepared runway was an advantage for military applications like giving the ability to drop troops in conflict areas.

To overcome the inefficiencies of rotary wing flight while maintaining the launch and recovery benefits afforded by VTOL, starting in the 1950's, aircraft manufacturers perused hybrid designs known as tilt-wing and tilt-rotor designs [7]. While helicopters are more mechanically complex than airplanes, tilt wing/rotor aircraft are significantly more complex than helicopters. The tilt wing design had wing mounted engines that would articulate vertically by rotating the entire wing (a type of which is depicted in Figure 4).

Figure 4: Boeing Vertol VZ-2 tilt wing [6]

Each rotor still maintains the complexity required of a helicopter rotor to conduct hovering flight [7]. The designs were difficult to pilot during the transitions from each mode of flight and while many manufacturers made prototype tilt wing designs, they have never been put into production [6]. The tilt rotor concept differs in that the rotors are mounted at the ends of the wing and only the rotors tilt during the transitional flight making the transitions more stable. The joint Bell/Boeing project, which started in 1983 to create the V-22 Osprey (Figure 5), was a success and finally in 1997 the aircraft was put into production for military applications [6].

Figure 5: V-22 Osprey in transitional flight [6]

The Osprey also relies on mechanically complex helicopter style rotors for orientation control while in hover or transitional flight.

Also starting in the 1950's, on a parallel track, aircraft manufacturers started to experiment with jet engine powered aircraft that would have VTOL capabilities. In Britain, Rolls Royce led the way in 1954 with their aircraft known has the thrust measuring rig which was an early test platform for jet powered VTOL (Figure 6) [8].

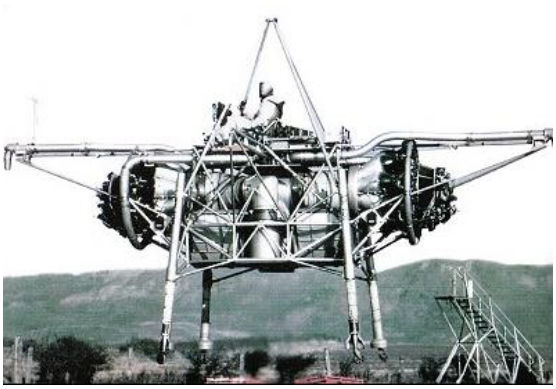

Figure 6: Rolls Royce thrust measuring rig [8]

Rolls Royce eventually produced Britain's first VTOL aircraft called the Short SC.1. The SC.1 used four vertically mounted engines for VTOL and a larger engine for forward flight [9]. Developments made on the SC.1 found their way through the experimental Hawker Siddeley P.1127 to the production Hawker Siddeley Harrier (known colloquially as the Harrier Jump Jet) [10]. The Harrier (Figure 7), uses thrust vectoring to generate lift in VTOL manoeuvres and a reaction control system (RCS) which is made of strategically placed jets used to control orientation [10].

Figure 7: Hawker Siddeley Harrier in VTOL mode [11]

Both the Osprey and Harrier are successful VTOL production aircraft that eliminate the dependence on undamaged runways for operational capability and enables operation from unprepared sites [9]. For military applications the advantages are clear.

2.1 Modeling and Control of Altitude

This section provides a background on models for rotor craft in modes relating to hovering and landing. Note that investigation of general models for aerial vehicles is beyond the scope of this thesis.

Much of the work in the area of autonomous hovering and landing has been completed on helicopter style VTOL UAVs. Fabiani et al. have shown successful use of a simple altitude controller in autonomous helicopters [12].

The system provides the option to use either a vertical velocity or altitude as a reference. The plant model is defined as a first order transfer function of the helicopters collective control in series with a first order transfer function that models the velocity response due to the collective control input. An integrator is used to relate the altitude to the vertical velocity. The altitude reference is received from a GPS; therefore autonomous landing would be difficult to achieve successfully due to absolute errors in the measurement.

A more detailed approach to autonomous helicopter landing has been described by Seong-Pil Kim et al. where the analysis was based on a helicopter with stable trimmed attitude [13]. The control law presented was a 2 degree of freedom (DOF) tracking control law which was shown to be globally stable using the Lyapunov stability theorem. While the paper specifically discusses autonomous landing, the experiment presented stopped short of actual touchdown (Figure 8) and it was considered future research.

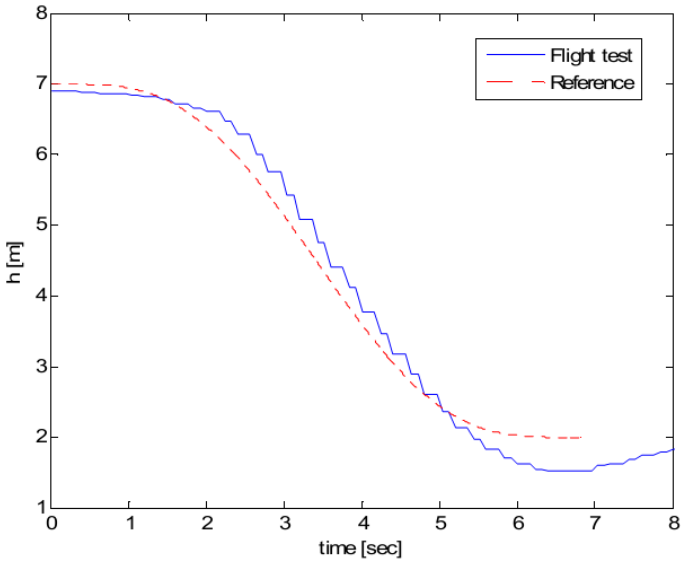

Figure 8: Altitude trajectory of autonomous helicopter landing [13]

The application of a differential global positioning system (DGPS) for positional measurement provided the required resolution to properly control the aircraft. Strategies for handling control into the ground effect were absent from the methodology presented. The conclusion was that the controller used for stable hover enables autonomous unmanned helicopter landing which had been demonstrated in flight.

The aforementioned work was loosely based on a paper by J. Kaloust et al. that presented a nonlinear controller for a 2-DOF helicopter model [14]. The work used Lyapunov's direct method to establish stability and used a recursive design technique to generate a controller. The method developed an approach that appropriately handles the nonlinearity experienced with large control inputs to the helicopters collective control.

Autonomous helicopter landing conducted by Saripalli et al. investigates vision based position control to hold the helicopter over the landing site [15]. The work includes no indication of what the circuit height altitude measurement device is; however, it does mention that an ultrasonic sensor is used near the ground. The autopilot altitude control has three modes called hover control, velocity control and sonar control. Target location is conducted under hover control and once centered over the target, the velocity control is enabled to conduct the descent. Once the sonar measurements are reliable enough, the autopilot switches to sonar control. The work shows the velocity and sonar controllers to be

simple PI controllers. The autonomous descent shown in Figure 9 shows a descent rate of 20cm/s after the landing target has been identified.

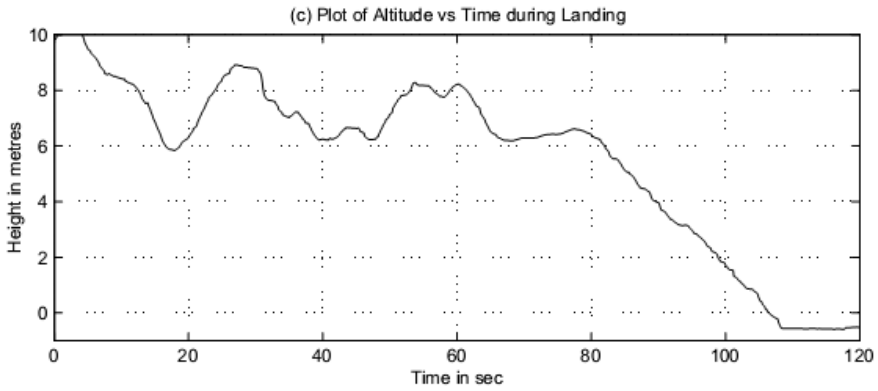

Figure 9: Autonomous descent of a vision based autonomous helicopter [15]

An altitude controller designed specifically for a four rotor flying robot is presented by D. Gurdan et al. that compensates for the altitude trim offset as the battery loses power [16]. The design describes using two controllers; one is based on the use of an accumulator that essentially acts as an integrator to slowly compensate for changes in the battery condition that will affect the neutral buoyancy throttle position. The second controller is capable of fast responses ideal for disturbance rejection and is implemented as a PD loop. The complete system is essentially a PID controller. The altitude feedback for this multi-rotor is received from an external motion tracking vision system.

All of the altitude models and control systems discussed in this section also rely on a stability control system used to maintain the aircrafts level orientation during descent. The next section discusses approaches used to achieve this required stability.

2.2 Stability and Control

A control system is also required to maintain the orientation and stability of a hovering aircraft in flight. This section describes background of some of the various approaches used to achieve this stability.

The approach to stabilization of a four rotor flying robot presented by D. Gurdan et al. uses a model free approach that requires tuning to achieve the desired performance [16]. The approach is unique in that it integrates the sum of the control input and gyro feedback. Integrating only the gyro feedback provides an orientation estimation that is subject to gyro drift and external disturbances. Their approach sums the control input to the gyro feedback before integrating to generate an orientation estimate that compensates for the drift. The overall control system would be considered a PID controller.

In the work of S. Bouabdallah et al., an approach to quad-rotor stabilization control is developed using a full Euler-Lagrange determined model of the system [17]. Investigation into system control using both a sliding-mode controller and back stepping controller were explored. It was found that back stepping control provided superior results to the sliding-mode control implementation. Note that these tests required the use of an external control computer communicating to the quad-rotor and that all the tests were conducted on a test stand with 3 degrees of freedom.

Also, in the work of B. Erginger and E. Altug great effort is put into generating a quad-rotor model [18]. However, the model was only used for simulation purposes and ultimately a PD controller was used for the orientation control while in simulation.

There are varied approaches that have been explored and tested in regards to VTOL aircraft stabilization. While it is clear there has been some advanced work in defining the system dynamics to generate realistic models, the control strategies seldom use a model based approach for control. While a range of processors have been applied to the control of these systems, it is clear that processing capability is a barrier to employing more advanced control schemes in flight. For practical UAV applications high speed processing increases weight and consumes more power which affects the aircrafts endurance rating. Also, ground based computing introduces latency into the control system which reduces control system bandwidth and has significant reliability implications due to the

nature of radio links. For practical implementation of UAV technologies on board computing and sensing is ideal and this requires implementation of effective and efficient control strategies.

Chapter 3
Experimental Design

Autonomous fixed-wing UAV recovery, the subject of this thesis, is predicated on electric propulsion to maintain controlled orientation and descent of the aircraft. The controlled descent of such an aerodynamic body diverges significantly from standard multi-rotor control by the necessity to conduct these manoeuvres far outside the intended operational envelope of the airframe. The control effort required to successfully complete an autonomous descent and landing can be studied in two parts. First would be the control of the orientation of the aircraft and second, the control of the aircraft translation in space relative to an inertial frame. For standard multi-rotor or helicopter control, orientation is used to directly control translational motion since the thrust vector is approximately fixed to the vertical axis of the aircraft's body frame. For vertical descent fixed-wing UAV recovery this topology leads to control difficulties related to disturbances generated by the aircraft's lift generating surfaces. The autonomous landing manoeuver requires that the aircraft counteract wind speed during the descent so that at the moment of touchdown there is zero ground speed. The natural consequence of this requirement is motion in the wind frame that acts on the lift generating surfaces of the UAV according to the angle of attack (α) and sideslip angle (β). Analyses of these forces which are beyond the scope of this thesis will be generally considered as disturbances affecting the system as shown in Figure 10.

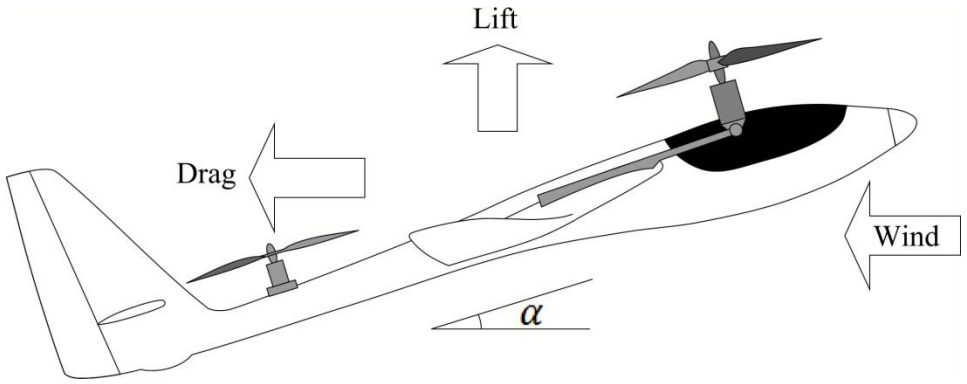

Figure 10: Wind generated disturbances acting on the Lux due to a high angle of attack

However, given that most fixed-wing UAV aircraft are statically stable (ie positive pitch and yaw stiffness), the aircraft's body frame will tend to align with the wind frame thereby subsequently

reducing these disturbances to zero as shown in Figure 11. This effect could be thought of as similar to a weather vane.

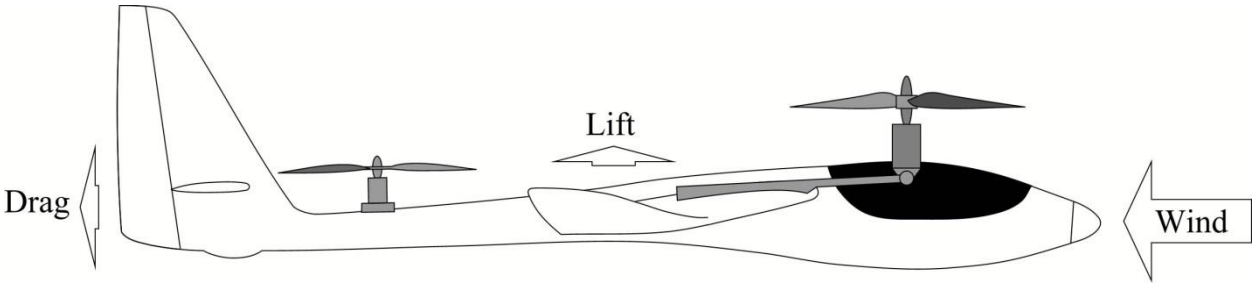

Figure 11: The Lux with small wind induced disturbances due to optimal orientation

To ensure there is minimal disturbance to the system, both the orientation and translation control schema must be designed to reduce actions that influence α or β away from zero. This can be achieved by the addition of thrust vectoring which adds a degree of freedom to independently control the orientation in the pitch axis, while also being able to move the aircraft in the fore and aft directions. In providing this degree of freedom, it is possible to maintain controllability and stability of the system that would otherwise be impossible in changing wind conditions.

The autonomous recovery system being explored also diverges from multi-rotor control given that the symmetry that simplifies the multi-rotor control system is not present when stabilizing a standard fix-wing airframe. Placement of the lifting motors to coincide with the existing airframe, the uneven distribution of mass and the uneven application of aerodynamic forces due to the aero-body, make stabilization a more challenging endeavour especially in the presence of atmospheric disturbance. Due to these circumstances, the control approach was separated into two interdependent analyses including the characterization and development of mathematical relations necessary to appropriately deal with them. Applied in series, within the auto pilot, these processes are executed sequentially as first control then mixing. The mixing controller is a type of decoupling controller applied between the controller and the plant as shown below in Figure 12.

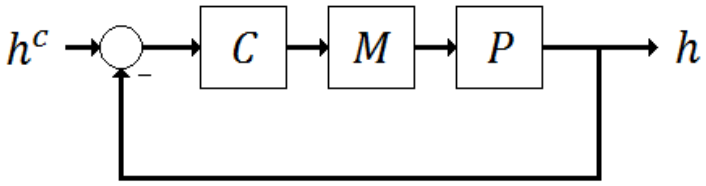

Figure 12: Altitude controller containing mixing controller (M)

This allows for the linear outputs of the controller to be fed into a mixer which applies the appropriate amount of input to the various actuators for a choreographed response that is balanced. Implementation of this scheme necessarily includes characterizing the system so that coordination of the actuators results in the system acting in a predictable manner. For instance, if the controller commands the system to increase lift, the system should be free from a coincident pitching and/or rolling tendency.

3.1 Experimental Airframe Development

In order to study the control aspects of autonomous recovery, an experimental aircraft was required that could facilitate the necessary data gathering experiments as well as test control hypotheses developed throughout the research process. To ensure that the research could eventually be applied to solving real world UAV recovery problems, it was prudent to experiment with typical UAV airframe topologies. Before implementation, the focus of airframe procurement was directed at using a sailplane style aircraft to modify for research purposes. Given that sailplanes have very high lift to drag ratios, they are often chosen as commercial UAV platforms for their high efficiency such as the CropCam UAV manufactured by MicroPilot [19].

A sailplane airframe made of Elapor foam was chosen as an experimental platform due to the fact that it would hold up to various levels of abuse given the durability of Elapor compared with airframes made of more rigid construction such as thin fiberglass shells. During the initial design phases mock-ups were used to test weight distribution and to find a configuration that would likely accommodate both the forward flight mode as well as the vertical descent. Once the proposed airframe topology was decided upon, the two main motors and tail motor were built upon a simple wood test frame that contained all the control devices including motor tilt actuators, electronic speed controllers, radio receiver, microcontroller based autopilot, inertial measurement unit (IMU) and lithium polymer (LiPo) battery. This enabled separate testing of the electric propulsion system for validation prior to integration with the airframe. Once the main electronic propulsion and control systems were tested, the test frame and sailplane were temporarily merged to ensure the proposed topology would be successful prior to designing and assembling the final airframe. This process was valuable for qualitatively determining the effect of the airframe, aerofoils and motor mounts within the wash developed by the motors being operated in their vertical position. While these effects are outside the scope of the thesis research, it was important to ensure the work done by the propulsion system was effective enough to generate the required lift while the aircraft was in descent mode. Positioning of the main motors was designed to strike a balance between applying lift near the center of gravity while ensuring the lift generating wash was somewhat unimpeded by the airframe components. This decision ensures the majority of the work in descent mode is being done efficiently by the main motors while the tail motor (which is dead weight in forward flight mode) is used mostly for pitch attitude control. The front profile view of the Lux can be seen in Figure 13 and shows the lateral position of the two main motors.

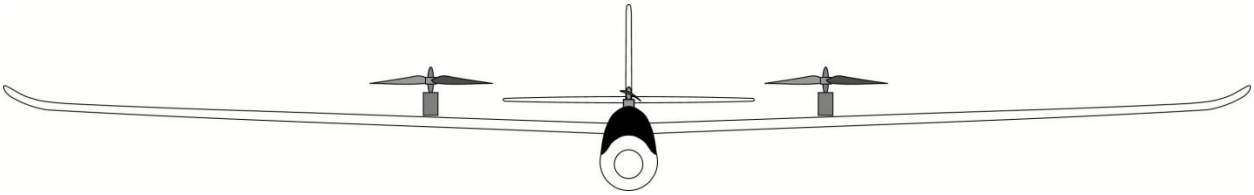

Figure 13: Front profile view of the Lux with motors in vertical orientation

The longitudinal position of the main and tail motors (in descent mode) can be seen below in Figure 14. In can also be seen in the figure where the prop wash of the main motors overlaps the leading edge of the wing and the motor nacelle.

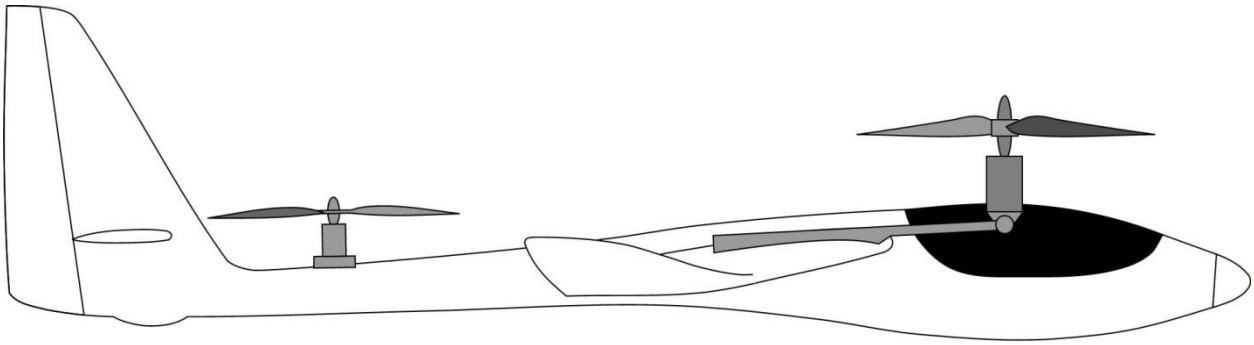

Figure 14: Side profile of the Lux indicating CG and lift distribution

Extensive testing to find the ideal position of the motors for UAV recovery was not conducted. The decision was pragmatic and based on both the issues mentioned above relating to balancing the center of gravity as well as structural considerations to mitigate the stress (such as wing twisting) of lifting the aircrafts weight in descent mode. The articulated main motors enable the Lux to operate in both vertical descent mode as well as forward flight mode as shown below in Figure 15.

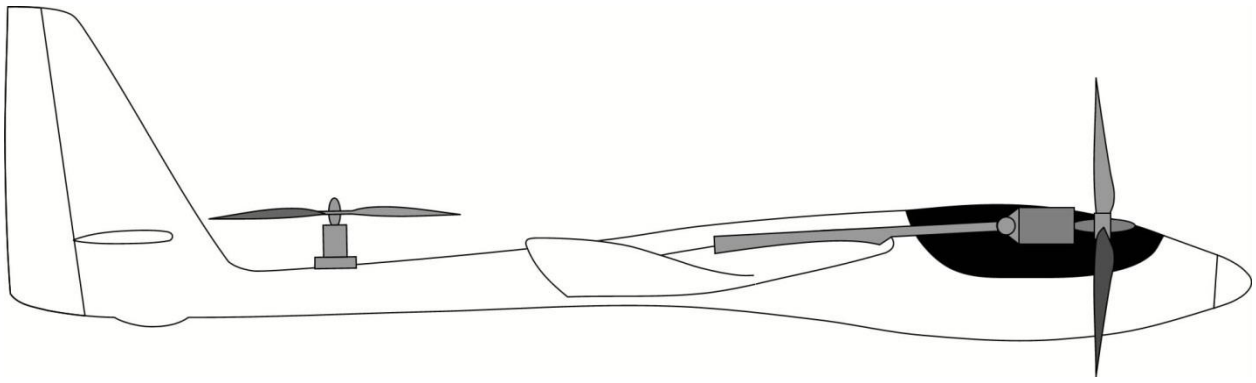

Figure 15: The Lux with main motors in forward flight mode

The articulating motor mounts designed to allow the Lux to convert between forward flight mode and vertical descent mode also provide the Lux with extra degrees of freedom for control. The Lux required the capability of accelerating forward and backwards without the pitching action that leads to instability that was discussed above. This problem was solved by employing the extra degree of freedom on each main motor to enable thrust vectoring. With the motors in the vertical position, it is possible to tilt them both fore (as shown in Figure 16) and aft which provides a mechanism for translation both forward and backwards.

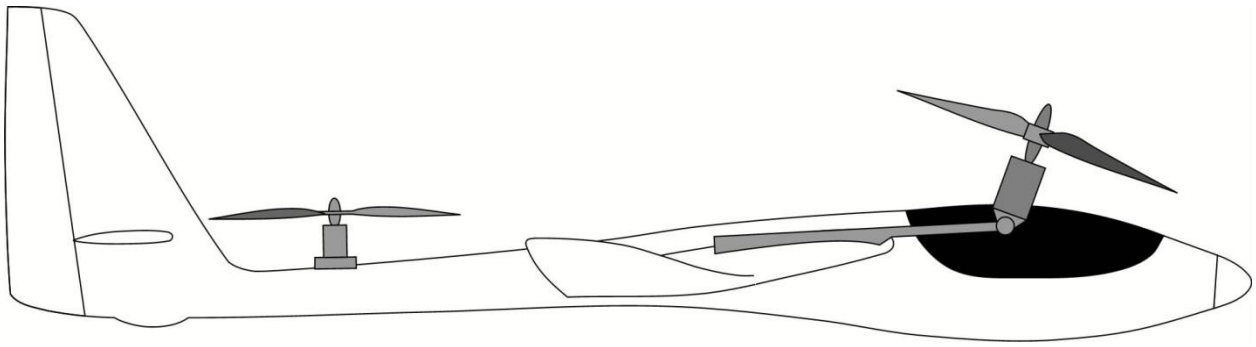

Figure 16: The Lux with main motors tilting forward to generate forward acceleration while descending

As well, in descent mode the heading of the aircraft can be controlled by tilting the motors in opposite directions as shown in Figure 17.

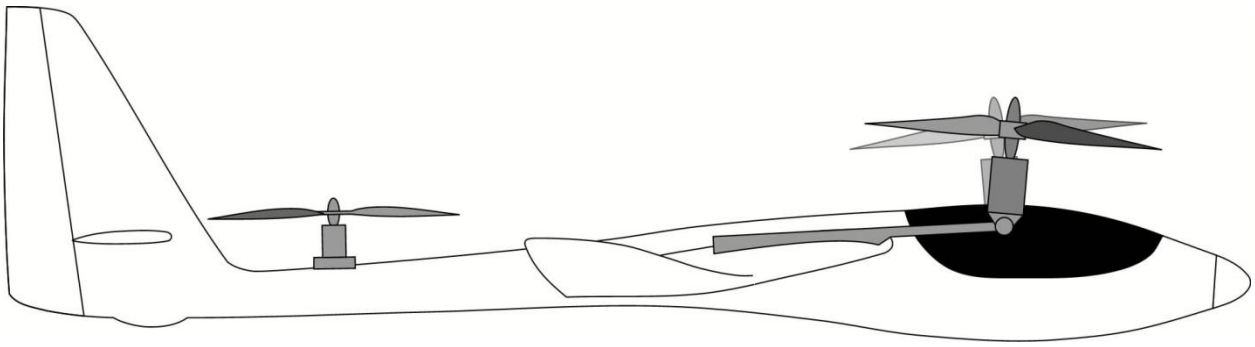

Figure 17: The Lux yaw control by articulating the main motors while descending

3.2 Control Experiment and Data Systems

To facilitate control research using the Lux, the aircraft was equipped with numerous sensors, control inputs and a data collection system. To coordinate the control and navigation operations using the available sensor data, the Lux was equipped with a custom twin processor autopilot. One processor, known as the flight controller, is mainly dedicated to interpreting external control references from either the navigation processor or the safety pilot, executing high bandwidth inner loop control using the inertial measurement unit (IMU), completing the required combined actuator mixing and generating the output signals. The other processor, the navigation processor, is responsible for interpreting the rest of the sensor data, executing navigation control as well as sending data to the ground station for collection. The Lux uses a suite of onboard sensors:

- IMU : data gathered from this sensor includes the rotation rate information (u, v, w) and orientation information (ϕ, θ, ψ)
- Ultrasonic range finder: provides distance above ground level (AGL)
- Barometric altimeter: provides a measure of the pressure altitude
- GPS : provides geo-referenced location information

Also, attached to the navigation processor is a data modem which is used to transmit pertinent data to a ground station for the purpose of data collection.

3.3 General Dynamic Equations and Decoupling Controller

The general dynamic equations for the UAV are described by [20],

$$F = I(q)\ddot{q} + h(q, \dot{q}) \tag{3.1}$$

where q represents the system states such as position, velocity, orientation and angular velocity, F represents the total forces and moments due to all the actuators, $I(q)\ddot{q}$ describes the inertial effects and h represents the gravitational, centripetal and wind induced drag forces applied to the body. In recovery mode the system is in a trimmed hover position where q_{ss} is the value of the states corresponding with the trimmed position and $\dot{q}_{ss} = 0$ giving,

$$h(q_{ss}, \dot{q}_{ss}) + F_{dist} = F_{ss} \tag{3.2}$$

where at steady state, F_{ss} is applied strictly to overcome gravitational effects. In the steady hover manoeuvre, disturbances to the system will be corrected by the control system simplifying 3.2,

$$h(q_{ss}, \dot{q}_{ss}) = F_{ss} \tag{3.3}$$

We are then left with,

$$I(\Delta q)\Delta\ddot{q} = F_{net} \tag{3.4}$$

where,

$$\Delta q = q - q_{ss} \tag{3.5}$$

And,

$$F_{net} = F - F_{ss} \tag{3.6}$$

We can find, in general, a decoupling controller M such that $MF_{net} = F_{decoupled}$ where M is designed to decouple the system dynamics [21]. In reality, this may only be possible at low frequencies and the higher frequencies that are not decoupled would be considered a disturbance that we reject with our control strategy. Hence, the strategy in this thesis is to decouple the system into a subsystem for orientation and a subsystem for altitude.

$$MJ(\Delta q)\Delta\ddot{q} = MF_{net} = F_{decoupled} \tag{3.7}$$

In general we don't know $J(\Delta q)$ or $h(q, \dot{q})$ so we will determine M experimentally to accomplish this decoupling. Henceforth, since M is essentially combining different actuator signals in order to accomplish this decoupling, the decoupling process will be referred to as mixing. This mixing is the topic of the next section.

3.4 Combined Actuator Characterization

Prior to working with the control aspects of the thesis, effort was put into system characterization required for mixing the output signals of the controller in order to decouple the system as described in the previous section. The most important aspect of coordinated actuator control was applying the correct throttle signals to the different motors to affect balanced lift. Applying the throttle signal alone must allow the Lux to generate lift that does not affect pitch or roll. The Lux's body axes i_b, j_b and k_b are defined in Figure 18 where p, q and r are angular velocities and L, M and N are applied moments in the roll, pitch and yaw directions respectively.

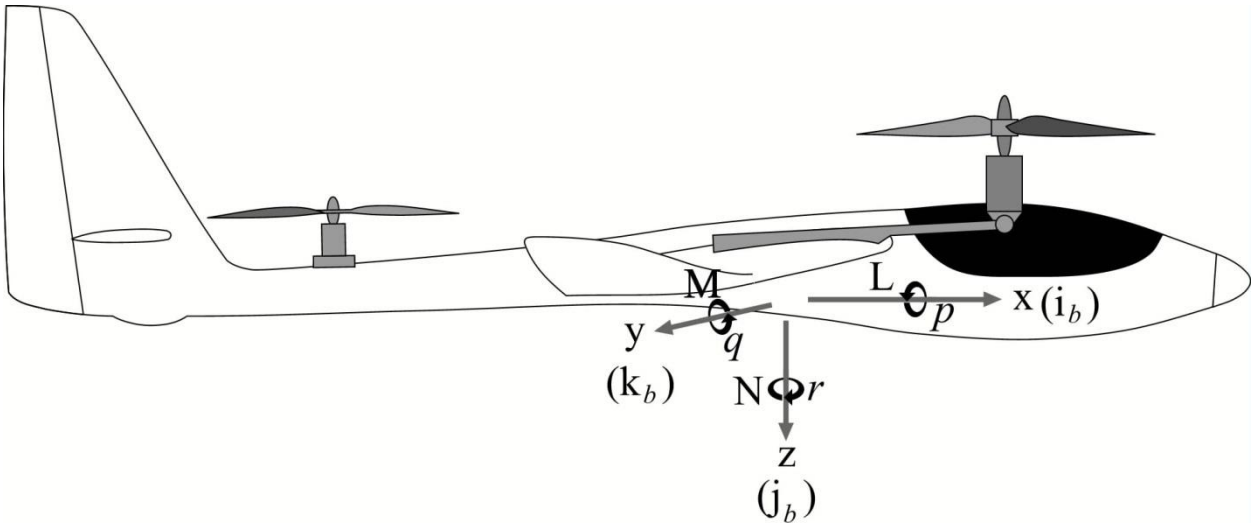

Figure 18: The body axes and angular velocities of the Lux defined

For a rigid body the inertia matrix is [22],

$$\boldsymbol{I} = \begin{bmatrix} \int (y^2 + z^2)dm & -\int xy\, dm & -\int xz\, dm \\ -\int xy\, dm & \int (x^2 + z^2)dm & -\int yz\, dm \\ -\int xz\, dm & -\int yz\, dm & \int (x^2 + y^2)dm \end{bmatrix} \triangleq \begin{bmatrix} I_x & -I_{xy} & -I_{xz} \\ -I_{xy} & I_y & -I_{yz} \\ -I_{xz} & -I_{yz} & I_z \end{bmatrix} \quad (3.8)$$

Since the Lux is built from a typical airplane configuration and the position of the motors maintain the standard aircraft lateral symmetry on the plane spanned by i_b and j_b we have $I_{xy} = I_{yz} = 0$. Then the moments of inertia matrix for the Lux is [23],

$$\boldsymbol{I} = \begin{bmatrix} I_x & 0 & -I_{xz} \\ 0 & I_y & 0 \\ -I_{xz} & 0 & I_z \end{bmatrix} \tag{3.9}$$

Given the inertia matrix it can be shown that the rigid body equations of motion are [24],

$$\begin{aligned} L &= I_x\dot{p} - I_{xz}\dot{r} + qr\left(I_z - I_y\right) - I_{xz}pq \\ M &= I_y\dot{q} - rp(I_x - I_z) + I_{xz}(p^2 - r^2) \\ N &= -I_{xz}\dot{p} + I_z\dot{r} + qr\left(I_y - I_x\right) - I_{xz}qr \end{aligned} \tag{3.10}$$

where L, M and N are respectively the rolling, pitching and yawing moments due to F_{net}. The rigid body equations define a system that has some longitudinal and lateral coupling. However, it has been shown that autopilots designed on the assumption of decoupled dynamics yield good performance [23]. We may therefore make the simplification at this time and present the system when the axes are principle [22],

$$\begin{aligned} L &= I_x\dot{p} - qr\left(I_y - I_z\right) \\ M &= I_y\dot{q} - rp(I_z - I_x) \\ N &= I_z\dot{r} - qr\left(I_x - I_y\right) \end{aligned} \tag{3.11}$$

The externally applied moments about the axes i_b, j_b and k_b are represented by L, M and N respectively. In descent mode, when neglecting aerodynamic body forces, the main externally applied moments are due to the rotor configuration. The rotor arrangement is shown below in Figure 19.

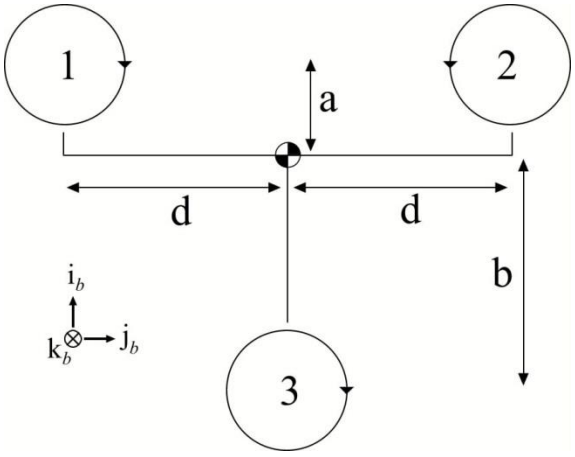

Figure 19: Top view of the Lux's rotor arrangement

This figure demonstrates that the main motors have lateral symmetry. Therefore a balanced application of throttle to motors 1 and 2 results in no net moment input, L. However, longitudinal symmetry does not exist shown also in Figure 20 below.

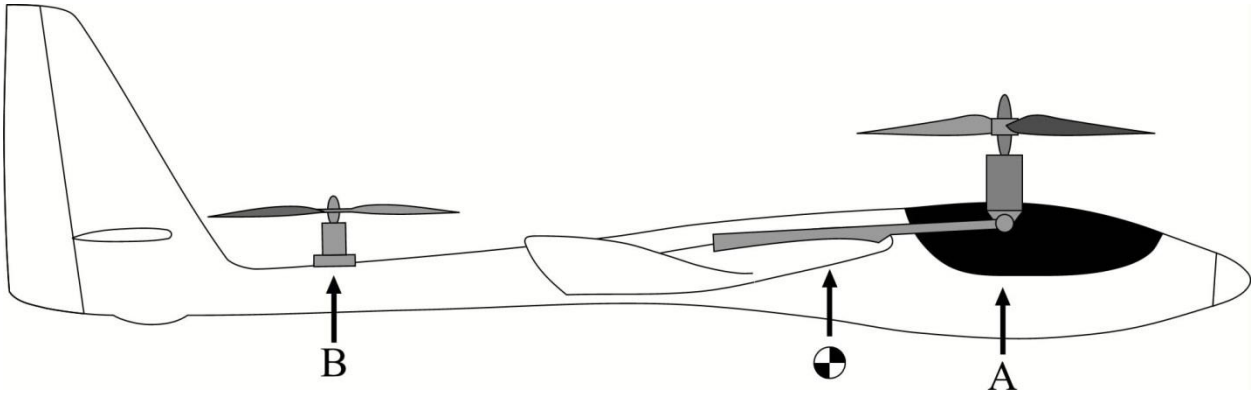

Figure 20: Applied thrust relative to the center of gravity

The main concern is ensuring throttle changes do not affect the pitch attitude. The longitudinal forces applied by the motors are shown in Figure 21.

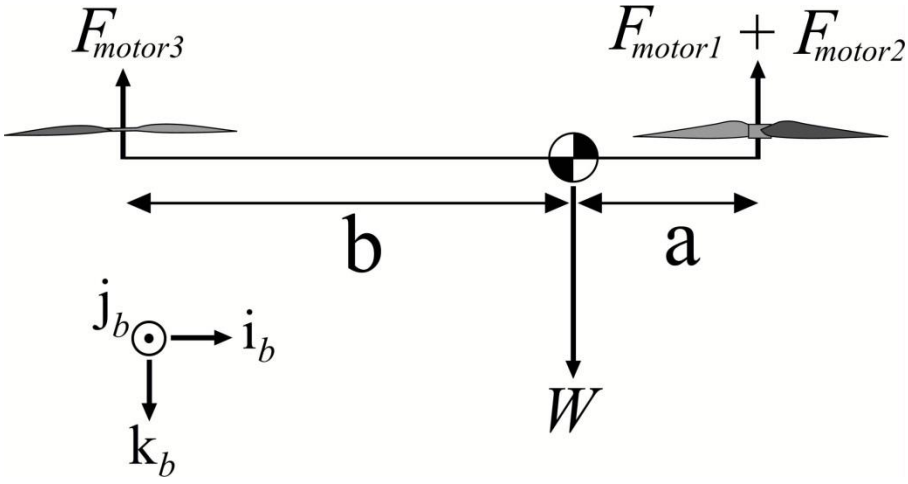

Figure 21: Longitudinally applied forces

3.5 Defining the Mixing Controller

Noting Figure 21 in the previous section, the pitch moment is described by,

$$L = (F_{motor1} + F_{motor2}) \cdot a - F_{motor3} b \tag{3.12}$$

The effect of the rotors thrust can be described by [23],

$$F_{motor1} = \frac{1}{2} \rho S_{prop1} C_{prop1} [(k_{motor1} \delta_t)^2 - V_a^2] \tag{3.13}$$

Where ρ is the air density, S_{prop} is the area swept by the prop, C_{prop} is the propellers lift coefficient, V_a is the airspeed incident on the propeller, δ_t is the throttle setting and k_{motor} is a gain that relates the throttle setting to the airspeed leaving the prop. The control signal, δ_t, applied to the motor controller is a pulse between 0 – 1000μs that relates to a motor RPM range. The value of k_{motor} is defined by setting the pulse lengths that define both the minimum and maximum RPM to correspond with the required propeller exit velocity airspeed.

In this application the forward speed of the prop in hover is negligible so 3.13 reduces to

$$F_{motor1} = \frac{1}{2} \rho S_{prop1} C_{prop1} (k_{motor1} \delta_t)^2 \tag{3.14}$$

The thrust generated by the main motors was graphed (Figure 22) and indeed the throttle to thrust relation is quadratic as shown on the trend line. However, it is also nearly linear over a generous region around the operating point where the total generated thrust matches the weight of the vehicle.

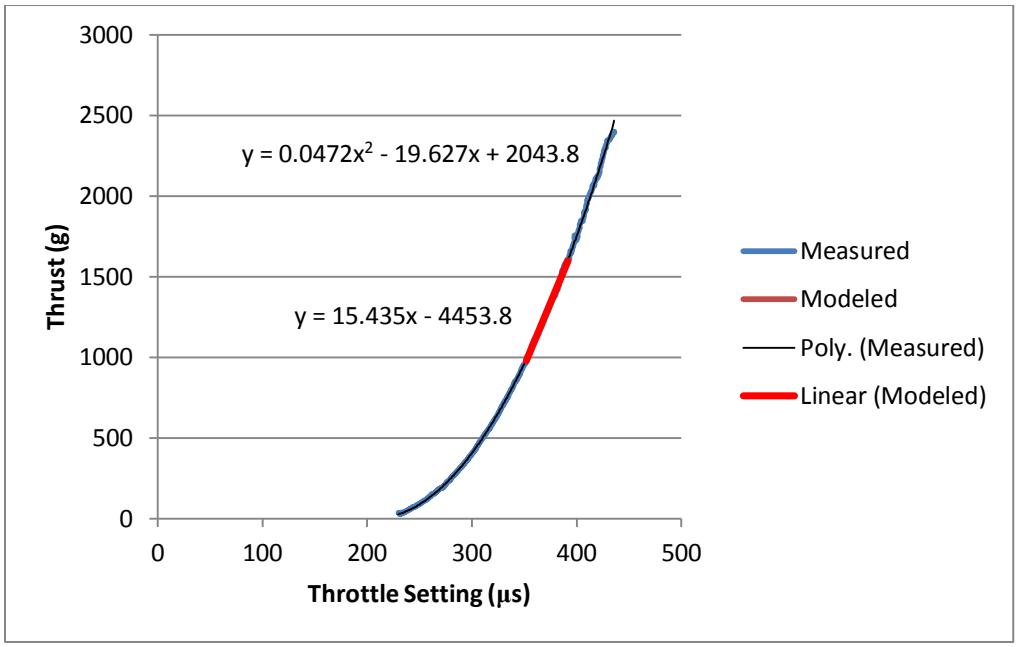

Figure 22: Lux main motor thrust vs throttle setting

While not completely necessary, the throttle was linearized around the operating point as shown. To balance the system, 3.15 and 3.16 were solved to find the trim position of each motor.

$$(F_{motor1} + F_{motor2}) \cdot a = 2F_{motor1} \cdot a = F_{motor3} b \tag{3.15}$$

$$F_{motor1} + F_{motor2} + F_{motor3} = W \tag{3.16}$$

Since k_{motor} is a programmable setting in the motor controller it can be adjusted to get the desired throttle response from each motor controller. For balanced lift it is required that,

$$\rho S_{prop1} C_{prop1} k_{motor1} \cdot a - \frac{1}{2} \rho S_{prop3} C_{prop3} k_{motor3} \cdot b = 0 \tag{3.17}$$

By solving 3.17 for k_{motor3} we have,

$$k_{motor3} = \frac{2S_{prop1}C_{prop1}k_{motor1} \cdot a}{S_{prop3}C_{prop3} \cdot b} \tag{3.18}$$

Then the system can be balanced by using the default value programmed into the motor controller for k_{motor1} to calculate the required k_{motor3}. The motor controller for motor 3 is then programmed with the appropriate k_{motor3} value.

To characterize the lift generating process including the effect of prop wash on the airframe, it was necessary to test the lift of each motor while attached to the airframe. The lift versus throttle data was gathered for both the main motors and the tail motor. Figure 23 below shows the generated thrust of the main motors and of the tail motor versus throttle setting where the throttle channel has 20 steps from minimum to maximum.

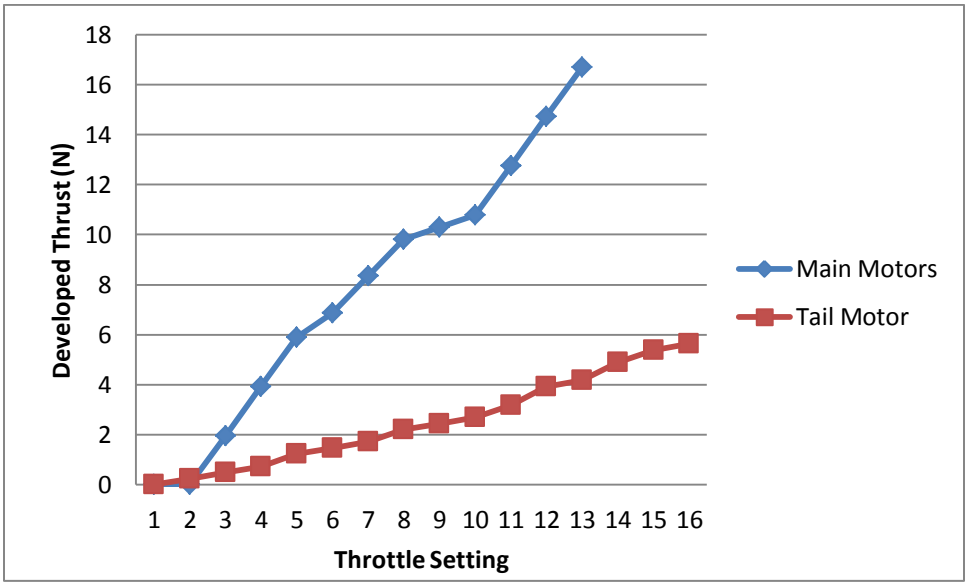

Figure 23: Main motor and tail motor thrust versus throttle setting

Data in the graph shows that the tail thrust is much lower than the thrust developed by the main motors and it is applied over a larger throttle input range. Given that the applied thrust is unevenly distributed from the airframes center of gravity, the data should be normalized to see what effect the

throttle will have on pitching the aircraft. Since the main motors apply thrust at point A as seen in Figure 21, which is 16cm from the CG point and the tail motor applies thrust at point B which is 50cm from the CG point the applied torque can be obtained by multiplying the generated thrust by the respective distance to the CG. Figure 24 shows the applied torque versus the throttle setting.

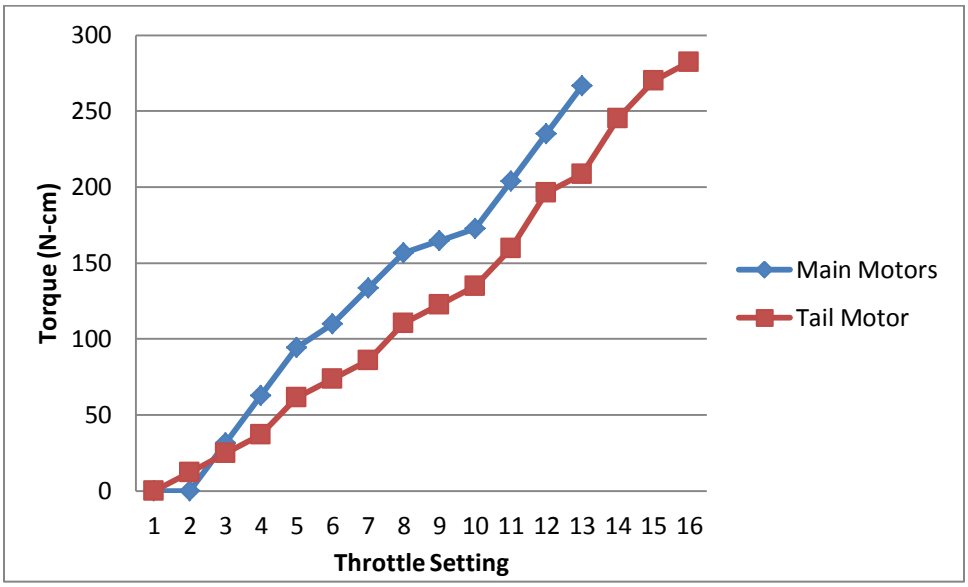

Figure 24: Generated torque versus throttle setting

These two applied torque data sets are reasonably matched and indicate the motors have been appropriately sized for relative efficiency. To provide a balanced thrust during descent one of the throttle signals will have to be scaled. By scaling the main motor throttle signal by 81.25% prior to applying it to the front motors a more balanced throttle scheme is created as shown in Figure 25 below.

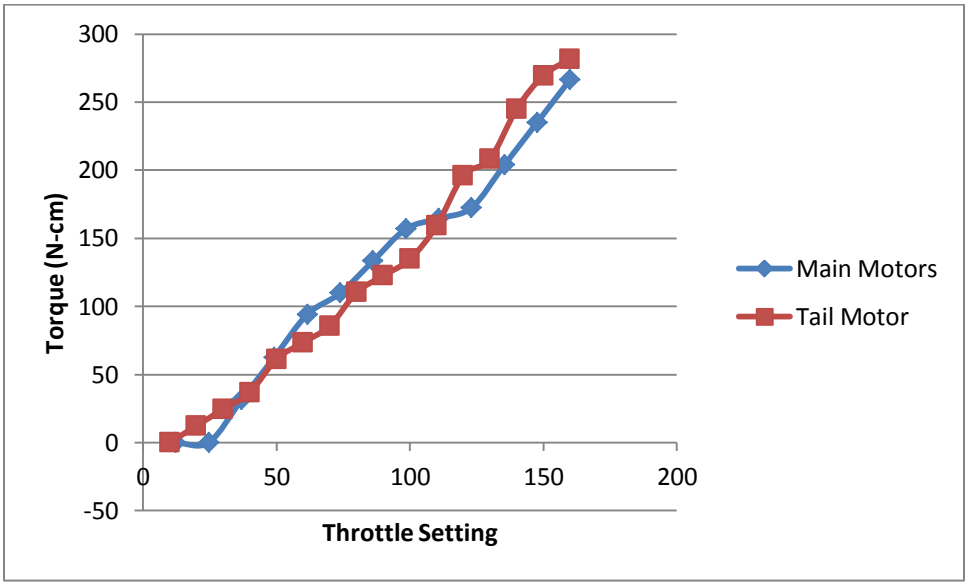

Figure 25: Torque versus throttle setting after applying scaling factor to main motors

One objective in the control scheme, to be discussed later, is to keep the aircraft pitch angle (θ) approximately zero to minimize the effect of velocity in the wind frame by keeping the angle of attack near zero. While θ is near zero, controller outputs to correct pitch (applied differentially to the main and tail motors) should be designed to not affect the total lift of the aircraft. To pitch the aircraft forward the tail throttle should be increased and the main motor throttles should be decreased in such a way that the total lift experienced by the aircraft remains constant. By comparing the thrust generated by the different motors (Figure 25) it can be seen that the thrust generated by the tail motor is approximately 30% of the main motor thrust across the calibrated throttle range. To prevent a net change of lift during the application of a pitch command the signal applied to the main motors must be -30% of that which is applied to the tail motor. Due to lateral symmetry, positioning commands around the roll axis (ϕ) using the two main motors will not lead to a net change in the lift when ϕ is approximately zero.

The success of the combined actuator characterization process was easily gauged by implementing the mixing within the autopilot. The autopilot was set into a manual mode that allows commands from a human safety pilot to control the aircraft via a radio transmitter. By hovering the Lux under manual control, it was clear that the mixing scheme was working. However, given that the hover is only operating the system within a very narrow throttle setting and the pilot has the ability to trim the aircraft at that throttle setting a secondary test was conducted to confirm the proper mixing was be

executed. The safety pilot was instructed to aggressively punch the throttle momentarily to see the reaction of the aircraft. Repeated tests demonstrated the Lux jumping straight up from the hover position without any pitch or roll tendencies' confirming the mixing strategies was working successfully.

Given that the Lux was built while carefully maintaining the CG at the position required for forward flight, there was very little doubt about whether the aircraft would be able to successfully achieve stable forward flight. Manual control flight tests with the motors in the forward flight positions confirmed the aircraft was stable and graceful in this mode of flight and exhibited no negative tendencies while flying. With the airframe fully tested and the actuator mixing working, the investigations and experimentation into autonomous recovery could now be initiated by further plant identification considering the aircraft response through the combined actuator control as a whole.

3.6 Altitude Control Trim Identification

In aircraft control systems, the trim position is the controller output when all the steady state errors are zero. For altitude control it is the throttle setting where the aircraft is neutrally buoyant. Compared with a proportional integral derivative (PID) control scheme, the trim position would be the output of the integrator when there is zero steady state error. With the altitude control of the Lux, it is desirable to know the throttle position that provides a steady unaccelerated hover to add the control effort to. Without knowing the proper trim or neutral throttle setting, the altitude error signal would have to get necessarily large before the aircraft could maintain a steady hover. To solve this problem with the addition of an integrator would not be appropriate for this application. As soon as the aircraft enters descent mode the controller requires the ability to stabilize the system without waiting for the integrator to settle to the trimmed position.

Using the data modem, it is possible to record the throttle values in flight and determine the throttle setting that provides a steady hover. The problem with this approach is that the throttle position for a steady hover changes during the flight according to the condition of the battery. As the battery charge is depleted the voltage starts to drop, this lower voltage requires a higher throttle setting applied to the motor controller to maintain motor RPM.

To solve the trim issue, the aircraft was strapped down to a lift indicating test platform and operated until the fully charged battery had been completely discharged. The battery voltage and throttle setting was recorded while the aircraft throttle was adjusted to maintain neutral buoyancy as indicated by the test stand. This test was completed five times and the results were aggregated to generate a battery voltage to throttle setting relation. Figure 26 below shows a graph of the results where the throttle setting is defined like other radio channels with a range of -100 to 100.

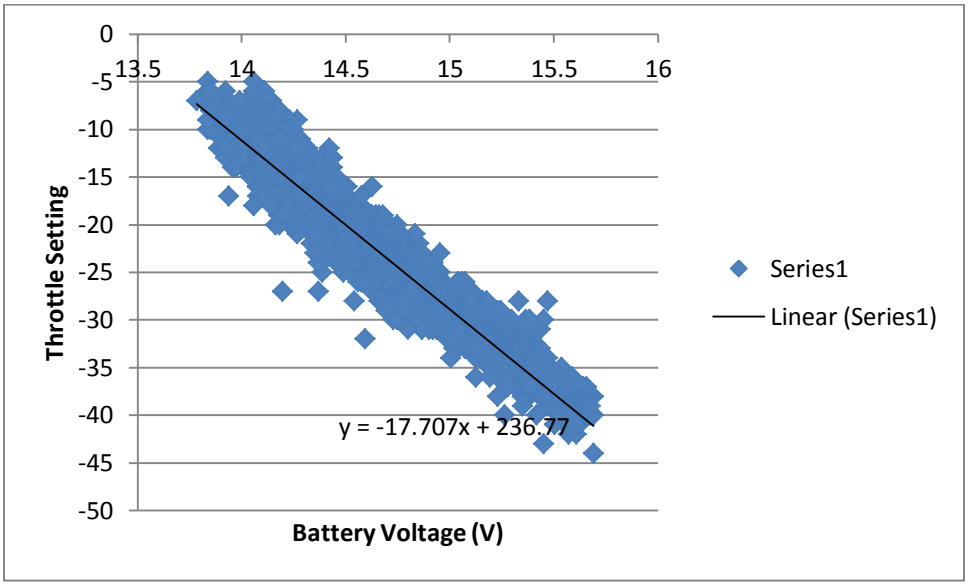

Figure 26: Throttle setting versus battery voltage

The trend line was used to generate the trim relationship. While the controller is operating in descent mode the battery voltage is continually sampled and the trim setting is updated to the output throttle command. Equation X below shows the throttle relationship with implemented trim.

$$\delta_t = \delta_t^* + \overline{\delta_t} = (-17.707 \cdot V_{batt} + 236.77) + \overline{\delta_t} \tag{3.19}$$

The total throttle command is the sum of the trimmed position, δ_t^* plus the required control effort as demanded by the linear controller.

3.7 Airframe Stabilization

While the Lux has built-in positive pitch, roll and yaw stiffness while in forward flight the vertical descent mode is inherently unstable. In fact, the vertical descent mode is impossible for the safety pilot to control without some added help from the autopilot. Rate mode is used to aid the manual piloting control by adding damping to reduce the speed of the system. Figure 27 below shows the basic rate mode configuration applied to the roll axis however both pitch and yaw axes have the same topology.

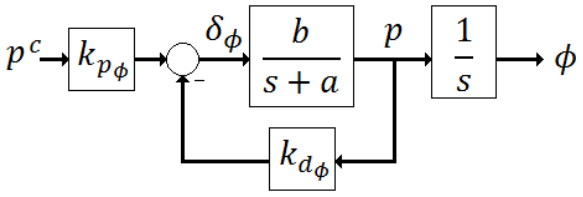

Figure 27: Rate mode configuration

In Figure 27, ϕ is the roll angle, p is the roll rate, δ_ϕ is the roll command applied to the plant and p^c is the commanded roll rate. The plant is represented by the first order transfer function and the integrator. The roll rate p is conveniently available as an IMU gyro signal. The rate feedback is multiplied by the derivative gain, k_{d_ϕ} and is then summed to the input signal provided by the pilot control. The gain k_{d_ϕ} is easily tuned during flight testing by increasing gain until the system starts to oscillate and then slightly backing off the gain until the oscillations stop. Note that the defined first order plant in theory would not exhibit this tendency; however, higher order dynamics come into play in practice. When properly tuned, the system counteracts external disturbances and requires more input from the pilot to generate the desired manoeuvres. Increasing the input gain allows the pilot control input to remain unaffected while still damping the system to any disturbances. Rate mode can be used as a manual control autopilot safety override should the autonomous system react unpredictably.

Orientation mode is built upon the rate mode topology. This mode can be used for autonomous flight as well as manual control and differs from rate mode in that the control input is an orientation command instead of a rate command. Figure 28 below shows the orientation mode configuration applied to the roll axis.

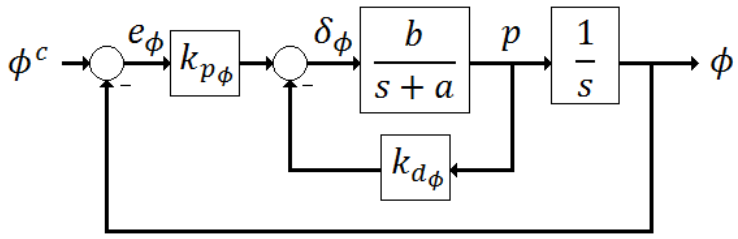

Figure 28: Orientation mode on the roll axis

In this mode the roll position ϕ is sampled from the IMU and subtracted from the commanded roll position ϕ^c to generate the error signal e_ϕ used to drive the inner rate loop discussed previously. The outer orientation loop is tuned by increasing the proportional gain k_{p_ϕ} until the system holds an upright orientation in flight without an external command signal. If k_{p_ϕ} is too large, oscillations are likely to develop indicating that either k_{p_ϕ} or k_{d_ϕ} should be turned down.

Orientation mode is also ideal for manual override control in emergency situations. The pilot's control input will be different from rate mode which is analogous to a standard helicopter control in that the stick positions map to axis orientations. Orientation mode benefits from the fact that if the pilot assumes manual control and loses the attitude of the aircraft due to poor visibility or unusual orientation simply releasing the control sticks will cause the aircraft to level out.

For the autonomous UAV recovery explored in this thesis, each axis is treated differently for stabilization purposes. The stabilization approaches for each axis is summarized in Table 1 below.

Table 1: Stabilization approaches of each axis

	Stabilization Mode	Input Command	k_d Setting
Roll (ϕ)	Orientation	From navigation controller	High
Pitch (θ)	Orientation	0 degrees	Medium
Yaw (ψ)	Rate	0 degrees/second	Low

The differences in stabilization approach for each axis is based on both the control strategy as well as the aircraft's configuration in descent mode. The roll axis is configured for orientation mode generally to maintain a level attitude during descent. If the landing scheme requires that the aircraft land at a particular point or is required to avoid known obstacles during the descent, the lateral direction of the aircraft can be influenced by the navigation controller by tilting the roll orientation as shown below in Figure 29.

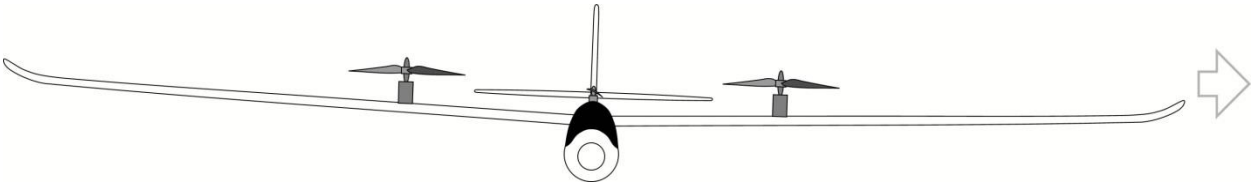

Figure 29: The Lux at a small roll angle to accelerate to the left.

Only a very small angle input for ϕ from the navigation controller is required to generate lateral accelerations due to the small side profile of the Lux. Because the Lux's long wings provide significant rotational damping around the roll axis, a high k_{d_ϕ} gain is required to counteract the plants mechanical damping when reacting to disturbances arising from unbalanced lift on the aerofoil.

As previously mentioned , in the presence of wind, angles of attack, α, that deviate from zero have a large undesirable influence on the altitude control stability. Therefore, to minimize this effect the body frame and the wind frame is aligned by keeping the pitch angle θ close to zero. There is very little mechanical damping on the pitch axis so k_{d_θ} must be high enough to damp out disturbances but not too high that oscillations develop. As mentioned earlier, if it is desirable to counteract wind drift in the longitudinal direction the main motors are articulated as shown in Figure 30 to provide the required force to counteract wind induced drag.

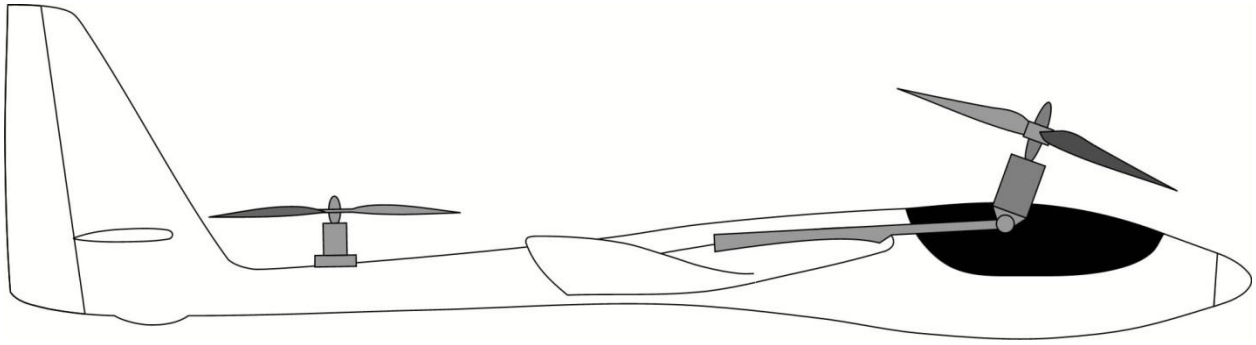

Figure 30: Articulated main motors for longitudinal thrust to overcome wind induced drag

The yaw axis is unique in that this application calls for the allowance of the yaw angle ψ to be susceptible to external disturbances, specifically wind. The control strategy during autonomous descent is designed around the Lux facing into the wind. Given the side profile shown in Figure 31, the vertical stabilizer that provides positive yaw stiffness in forward flight is also effective at keeping the lux facing into the wind during the descent manoeuver.

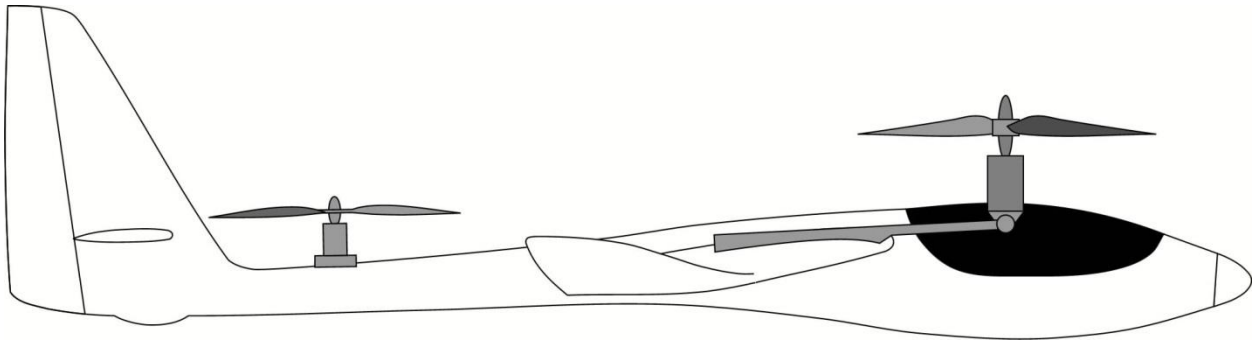

Figure 31: The Lux side profile showing the fin area responsible for positive yaw stiffness

By having the yaw axis in rate mode with an input of zero, the aircraft is damped in the yaw rotation but is able to slowly weather vane into the wind during descent without employing other control effort.

The application of the system decoupling and stabilization techniques provided in this chapter is designed to keep the aircraft stable when in the vertical descent mode. Ultimately the control actions keep the aircraft in an orientation designed to minimize the angle of attack α and sideslip angle β which reduces aerodynamic forces that could destabilize the system if unaccounted for. This hovering attitude allows the altitude to be controlled as if decoupled from the aircrafts orientation.

The analysis that follows in this thesis is predicated upon the controlled orientation described in this chapter.

Chapter 4
Altitude Control

The focus of this thesis was handling the vertical descent control. In previous chapters, prerequisites to the altitude control such as airframe design, actuator mixing and stabilization were discussed. These items are critical to the system and once completed, define the system that will have its altitude controlled for autonomous UAV recovery. To effectively control the aircrafts altitude in descent mode is not a trivial matter for a couple reasons. The thrust required for descent is roughly five times greater than what would be considered the maximum required for forward flight. In descent mode, the majority of this thrust generated by the aircrafts propulsion system is used to support the weight of the aircraft. Simply increasing the thrust required to achieve neutral buoyancy on the Lux by 1% (a throttle resolution of 3 steps) induces a vertical velocity of approximately 60cm/s. This small input generating large outputs is still reasonably controllable under ideal conditions but depends on good quality data about the altitude state. System disturbances have considerable effects on the altitude control which cannot be ignored. As noted, the aero-body generates significant forces under the influence of wind. The thrust of the propellers is dependent on the propeller aerofoil angle of attack. Changing winds affect this angle of attack leading to varying lift and increased altitude control difficulty.

4.1 Altitude Measurement

Reliable sensor data is critical to properly control the altitude. The common sensors for this task include GPS, barometric altimeter, ultrasonic range finder, laser range finder. Each of these sensors has different accuracies, resolutions and ranges that affect their ability to provide reasonable data for autonomous UAV recovery. Table 2 below shows typical values for these common UAV altitude sensors.

Table 2: Typical accuracies and resolutions for common UAV altitude sensors

	Typical accuracy	Typical resolution	Range considered for application
GPS	+/- 15m	0.1m	Unlimited
Barometric altimeter	0.1m	0.01m	Unlimited
Ultrasonic range finder	0.05m	0.01m	3-6m
Laser range finder	1m	0.1m	Unlimited

Note that the barometric altimeter's accuracy is measured in pressure altitude. Its absolute accuracy is not defined since atmospheric conditions affect barometric pressure leading to changes in the measured pressure altitude. Due to resolution and accuracy considerations, the ultrasonic and pressure altimeter were chosen as control inputs. As mentioned previously, the pressure altimeter is employed during the descent from circuit height to near ground level. When the UAV is near the ground the ultrasonic sensor readings are used for feedback.

The barometric altimeter's pressure altitude slowly drifts with changes in atmospheric conditions as shown below in Figure 32.

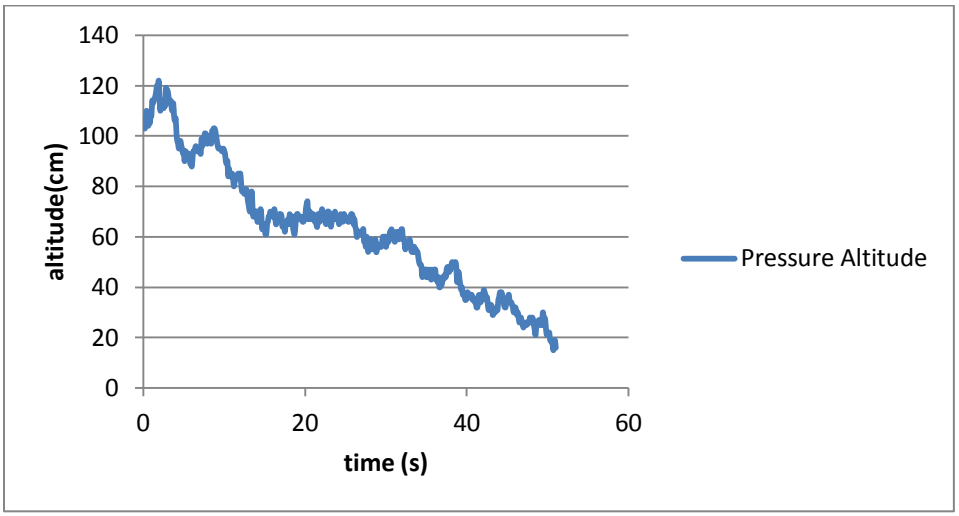

Figure 32: Pressure altitude drifting over time while UAV altitude is fixed

To demonstrate the negligible effect of this drift the same data was overlaid upon a simulated descent from 10m at a moderate descent rate of 40cm/s as shown in Figure 33 below.

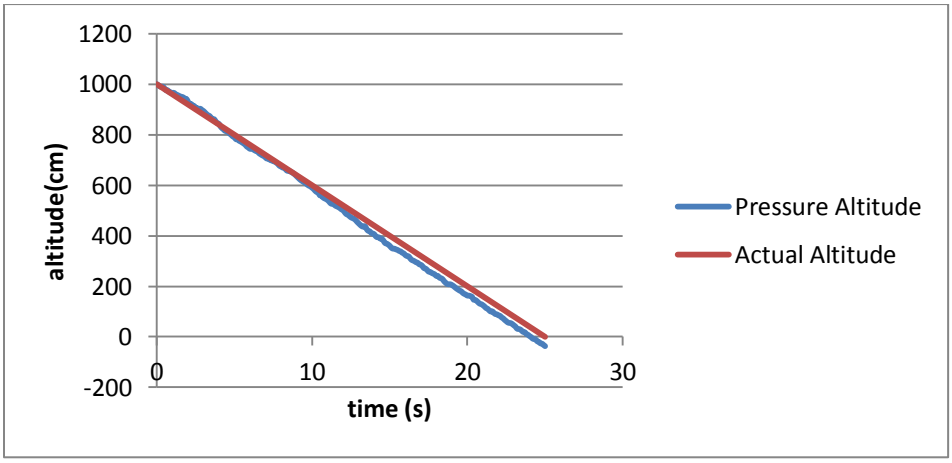

Figure 33: Simulated descent experiment showing pressure altitude drift

This demonstrates that although the pressure altitude drifts over time, it is still possible to use the barometric altimeter as decent measurement feedback device. Over the simulated descent using real pressure data, the altitude error at the end was 37cm. Important is that this sensor is used during stage

1 of the descent manoeuvre where the controller is controlling vertical velocity so sensor errors affect the desired rate of descent. The drift in barometric pressure in the above simulation amounts to an average measured descent rate of 41.48cm/s instead of the actual 40cm/s rate that was desired. This small error is acceptable and is likely to be smaller than the effect of atmospheric disturbances buffeting the aircraft.

For the most part, when the UAV is below 3m the sonar measured altitude data can be taken as correct. Small deviations occur due to changes in the speed of sound however for the application these minute differences do not affect the results. There is the occasional false ping received as shown below in Figure 34.

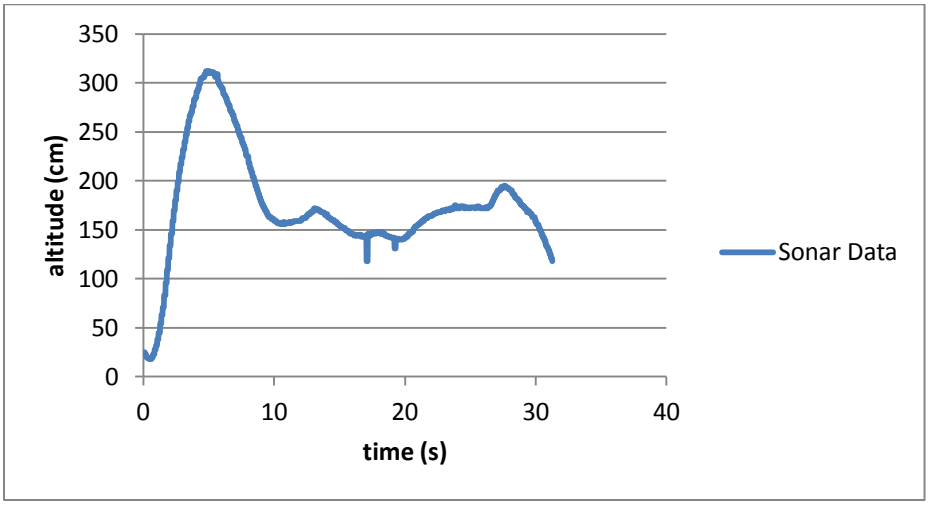

Figure 34: Sonar data showing the reception of false pings

These errors are not typical and many flights can be made without experiencing a single error. The control approach however must anticipate such errors to ensure robustness under varying conditions.

4.2 System Identification

Before attempting to characterize the plant, it was necessary to decide on the control objectives and the control approach to meet those objectives. The two unique applications of altitude control during autonomous recovery is the initial descent using the barometric altimeter as feedback and the landing flare, where the aircraft is decelerated, using the ultrasonic rangefinder as feedback. These two stages of the descent need to control the rate of descent and altitude AGL respectively. Therefore, the state space system should track both the altitude and vertical velocity so that these states can be easily monitored and controlled.

To define a simple system that tracks both vertical velocity and the altitude as states, it was desirable to define the plant as a second order system including an integrator. Referring to 3.1 to 3.7 it is expected that there would be one pole at the origin and the other pole would be a function of the systems damping. This simplified system enables the use of modern control theory within the limited processing capability of the autopilot. To characterize the system using a least squares identification algorithm, it was necessary to first stabilize the system since open loop operation of the aircraft is unstable. Employing a simple closed loop proportional controller prevents the aircraft from flying too high or too low during the characterization process. The control loop is shown below in Figure 35 where h is the altitude, $\dot{h}$ is the vertical velocity, and h^c is the commanded altitude.

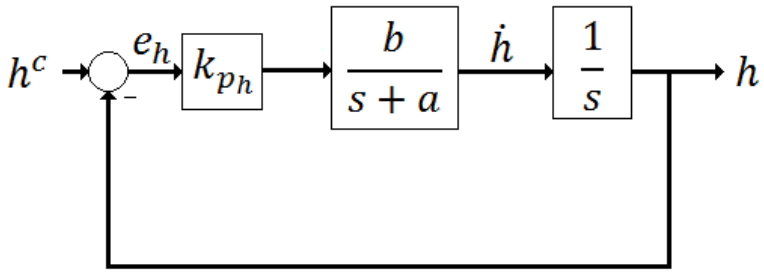

Figure 35: Proportional control loop used to stabilize the system

The closed loop transfer function of this system is,

$$\frac{h}{h^c} = \frac{k_{p_h} b}{s^2 + as + k_{p_h} b} = \frac{n_0}{s^2 + d_1 s + d_0} \tag{4.1}$$

To identify the plant using Matlab, the system must be defined as a second order model with no zeros. Using the identified transfer function, the second order plant model including the integrator, can be extracted from the resultant system equation. In this case,

$$b = \frac{n_0}{k_{p_h}} \tag{4.2}$$

$$a = d_1 \tag{4.3}$$

For this identification technique to work and provide the desired plant it is a necessity that $n_0 \approx d_0$. If this requirement is not met then the second order transfer function including integrator will not be the form identified. The system identification experiment was executed by exciting the system using a pseudo random input as shown in Figure 36.

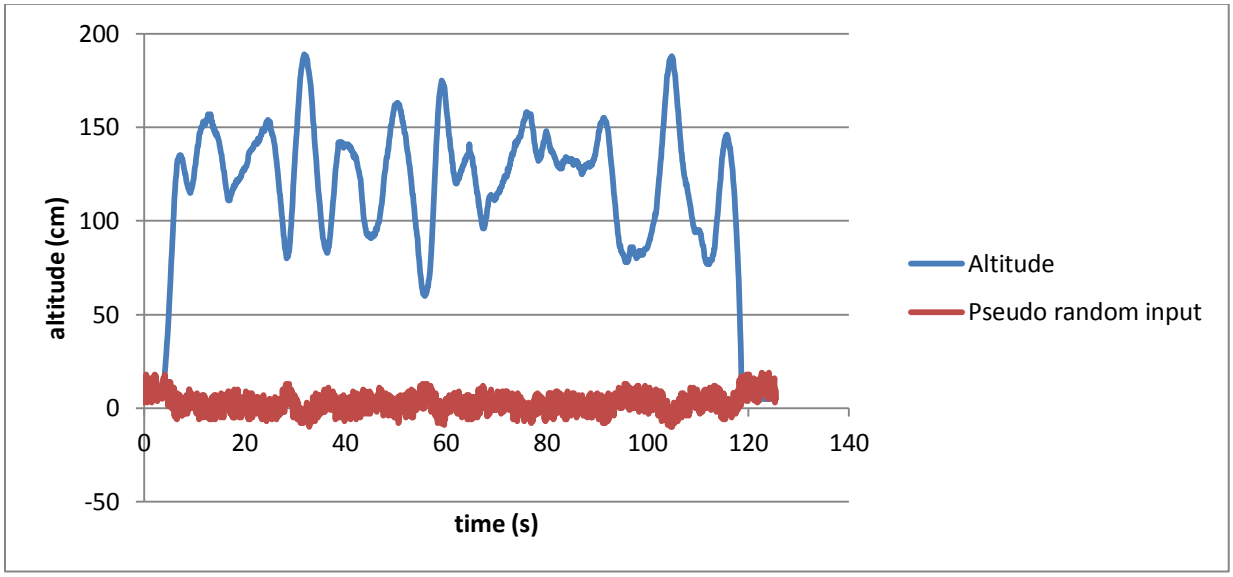

Figure 36: System identification experiment using pseudo-random excitation

The data was used to generate a transfer function that best fit the data as shown below in Figure 37. The resulting transfer function received was,

$$\frac{h}{h^c} = \frac{0.5936}{s^2 + 0.2138s + 0.5041} \tag{4.4}$$

For the system identification experiment $k_{p_h} = 0.8$, therefore if we assume the $n_0 \approx d_0$ condition is met we have,

$$b = \frac{0.5936}{0.8} = 0.742 \tag{4.5}$$

$$a = 0.2138 \tag{4.6}$$

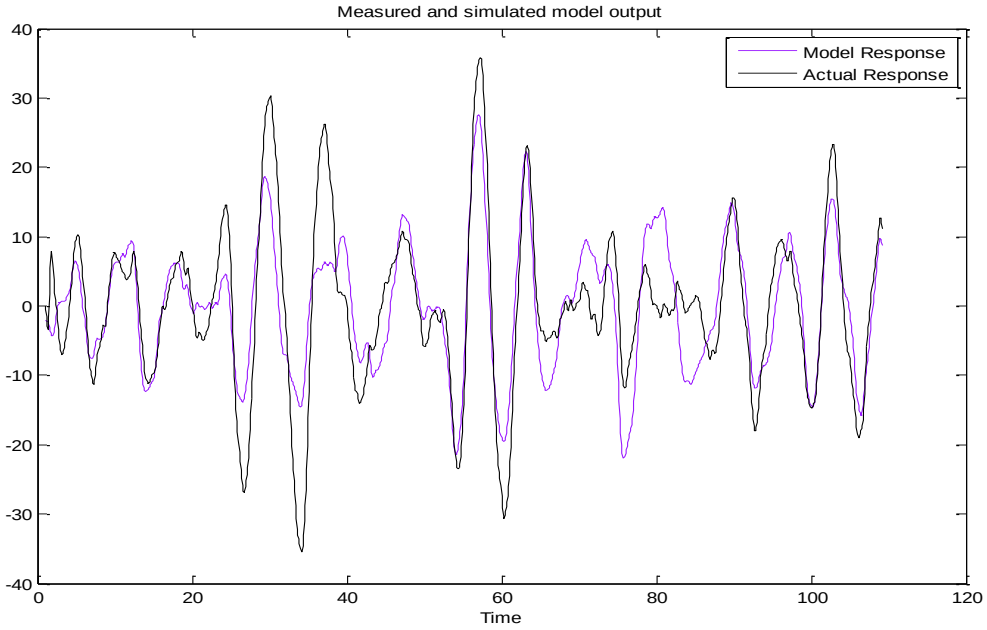

Figure 37: System identification results

This would provide an internal transfer function of,

$$\frac{\dot{h}}{\delta_t} = \frac{b}{s + a} = \frac{0.742}{s + 0.2138} \tag{4.7}$$

Unfortunately, this transfer function provides a steady state gain of 3.47 where experimental evidence gathered from fixing the throttle and measuring the corresponding steady state vertical velocity, has shown that the actual gain of the system is approximately 20.

Seeking a more suitable model, a second approach was tested to characterize the system. The first order response from throttle to vertical velocity was investigated through a series of experiments. The aircraft was set to hover using a manually tuned PD controller. Once stabilized and settled, a step input was provided to the throttle while recording the response of the altitude state. The typical response can be seen in below Figure 38.

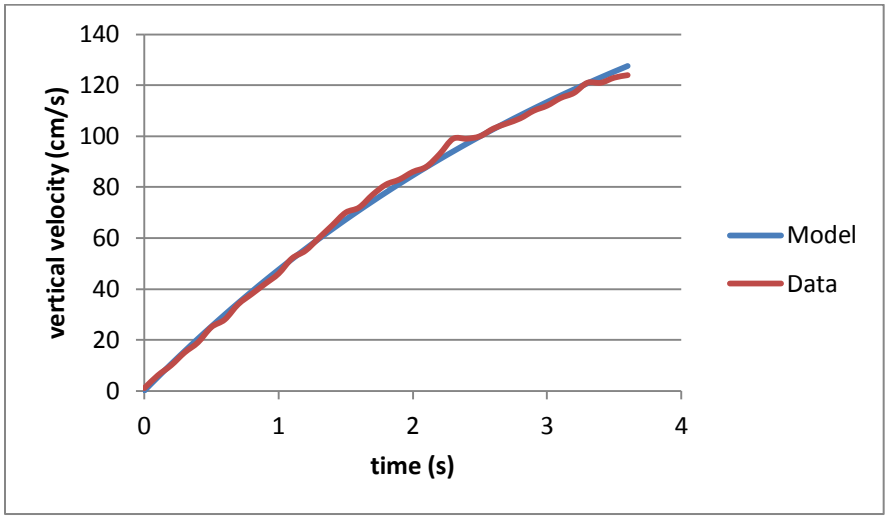

Figure 38: Measured and modeled first order response

After filtering and fitting the data the following transfer function was obtained.

$$\frac{\dot{h}}{\delta_t} = \frac{5.375}{s + 0.25} \tag{4.8}$$

Given the steady state gain for this transfer function is 21.5, these results are in agreement with earlier tests that indicated the steady state gain was approximately 20. Interestingly, the pole location of this identified plant is close to the pole location identified in the plant of 4.7.

Using the transfer function 4.8 and adding the integrator gives the plant model,

$$\frac{h}{\delta_t} = \frac{5.375}{s^s + 0.25s} \tag{4.9}$$

Which can be converted into a state-space representation that preserves the states $\dot{h}$ and h,

$$\begin{gathered} \dot{x} = \tilde{A}x + \tilde{B}\delta_t \\ \dot{x} = \begin{bmatrix} 0 & 1 \\ 0 & -0.25 \end{bmatrix} x + \begin{bmatrix} 0 \\ 5.375 \end{bmatrix} \delta_t \\ x = \begin{bmatrix} h \\ \dot{h} \end{bmatrix} \end{gathered} \tag{4.10}$$

In order to generate reliable state data for this control, it was decided to employ a Kalman filter [25]. The system was discretized using the forward Euler approximation and a sampling time of 0.1s to get,

$$\begin{gathered} \dot{x}_k = Ax_{k-1} + B\delta_{t_{k-1}} \\ \dot{x}_k = \begin{bmatrix} 1 & 0.1 \\ 0 & 0.975 \end{bmatrix} x_{k-1} + \begin{bmatrix} 0 \\ 0.5375 \end{bmatrix} \delta_{t_{k-1}} \end{gathered} \tag{4.11}$$

The discrete Kalman filter time update is applied [25] which in this application is used predict the altitude related states from the known throttle setting $\overline{\delta_t}$ and the identified process equation,

$$\hat{x}_k^- = A\hat{x}_{k-1} + B\delta_{t_{k-1}} \tag{4.12}$$

$$P_k^- = AP_{k-1}A^T + Q \tag{4.13}$$

Here P_k^- is the $a\ priori$ estimation error covariance and P_{k-1} is the $a\ posteriori$ estimate error covariance determined in the previous step $(k-1)$ as in 4.16 and Q is the process noise covariance [25]. The Kalman filter measurement update is applied [25] which uses the altitude measurement to correct the predicted states.

$$K_k = P_k^- H^T (HP_k^- H + R)^{-1} \tag{4.14}$$

$$\hat{x}_k = \hat{x}_k^- + K_k(z_k - H\hat{x}_k^-) \tag{4.15}$$

$$P_k = (I - K_K H)P_k^- \tag{4.16}$$

The objective of the Kalman filter is to reduce the $a\ posteriori$ estimate error P_k. In Equation 4.15 the residual, $(z_k - H\hat{x}_k^-)$ represents the difference between the measured and predicted states. The value of K_k calculated in 4.14 results in the minimizing of P_k when applied to the residual in 4.15 [25].

The Kalman filter matrix equations were converted into a sequence of single line equations that could be executed within the autopilots 16-bit microcontroller for in flight execution. Captured sensor data was evaluated to determine the variance of the measured signals in order to generate the R matrix. Note that since the system has two altitude measuring devices the R matrix needs to be changed according to the sensor noise covariance of the particular sensor currently in use. In practical applications, the determination of the Q matrix is difficult to determine and so the process noise ends up being attributed mostly due to plant uncertainty [25]. Therefore, the Q matrix values were chosen based on the results from simulations that were run using actual flight data. This was achieved by adjusting the variance associated with the throttle to vertical velocity transfer function until the estimate closely agreed with the measured data. Below in Figure 39, the comparison between the actual and filtered data is displayed.

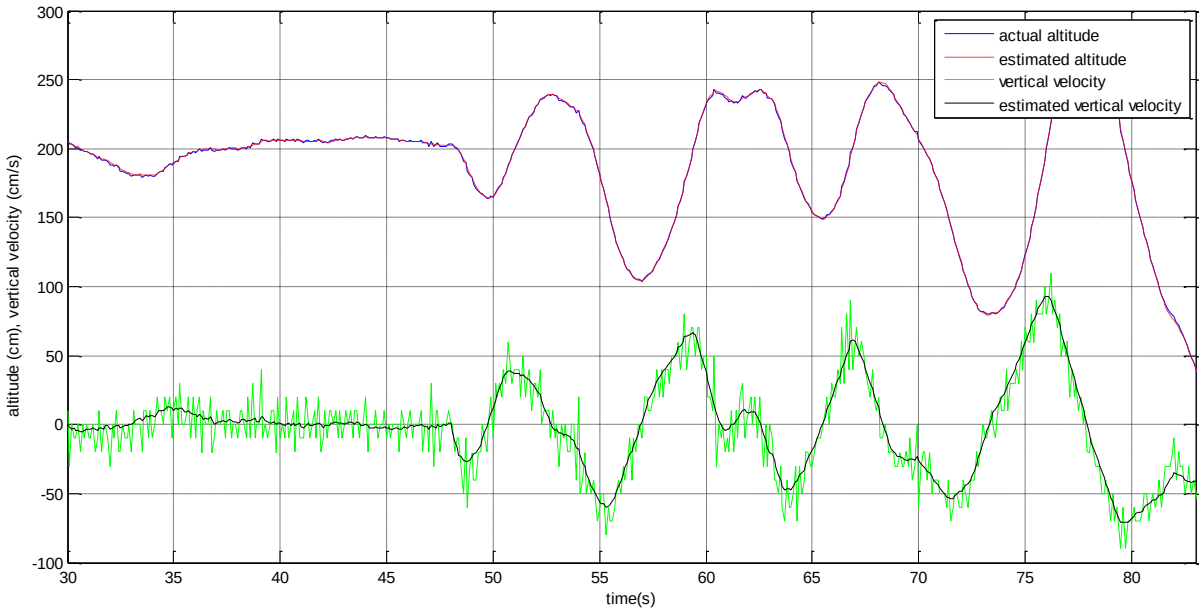

Figure 39: Comparison of results between actual and Kalman filtered altitude related states

The first half of the flight is stabilized using a simple manually tuned PD controller while the second half is flight under safety pilot control. The flight shown uses the more accurate sonar for altitude measurement so that the altitude state does not benefit from the filtering as much as the vertical velocity state. The quality of the filtered vertical velocity compared with that which was derived from the altitude measurement confirms the identified plant is a reasonable approximation.

4.3 Controller Design

In designing the controller, the system model was entered into simulation to develop and experiment with a suitable altitude control scheme. Given the state feedback from the Kalman filter, a linear quadratic regulator (LQR) controller seemed to be an ideal candidate for controlling the Lux's altitude. Note, this section of the thesis uses matrices Q, R, K and P which are distinct from the matrices presented in the previous section with Kalman filtering and are reused because they are traditionally used when presenting an LQR control system. Since an LQR is an optimal control system, it is designed to provide a minimum performance index where in this case the performance index is,

$$J = \int_0^\infty \left(x^t Q x + {\delta_t}^t R \delta_t\right) dt \tag{4.17}$$

where Q and R, used to penalize the state vector and control signals, are positive semi definite and positive definite respectively. In the plant model that is the subject of this thesis the two states being tracked is the altitude h and vertical velocity $\dot{h}$ while the control input is the throttle δ_t. The choice of Q and R can be defined as [24],

$$Q = \begin{bmatrix} \frac{1}{h_{max}^2} & 0 \\ 0 & \frac{1}{\dot{h}_{max}^2} \end{bmatrix} \tag{4.18}$$

$$R = \frac{1}{{\delta_t}_{max}^2}$$

Where h_{max} is the maximum desired altitude, $\dot{h}_{max}$ is the maximum desired vertical velocity and $\delta_{t_{max}}$ is the maximum desired throttle input [24].

The performance index in 4.17 is minimized when [26],

$$K = R^{-1}B^T P \tag{4.19}$$

Where, P is a $n \times n$ matrix which is found by solving the algebraic Riccati equation [26],

$$A^T P + PA - PBR^{-1}BP = -Q \tag{4.20}$$

For the LQR used to control this system the control law is given by,

$$\delta_t = -Kx = -(R^{-1}B^T P)x \tag{4.21}$$

A block diagram of the system is shown below in Figure 40.

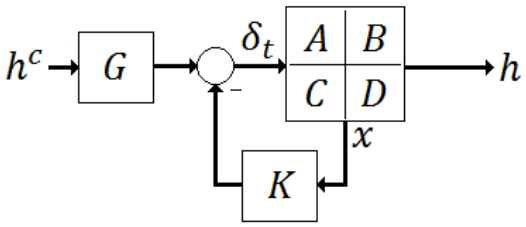

Figure 40: LQR controller applied to altitude control

Note that the state feedback shown is derived from the Kalman filter and can be shown to be optimal according to the separation principle [26]. The complete system is now,

$$\begin{aligned} \dot{x} &= (A - BK)x + BGr \\ y &= Cx \end{aligned} \tag{4.22}$$

Since the control law K has been defined, all that remains to be determined is the value G to appropriately turn the altitude command into a form that will properly control the new state feedback system. In the absence of a disturbance it is desired to have zero steady state error which means,

$$y_{ss} = \lim_{t \to \infty} y = r \tag{4.23}$$

Since,

$$\dot{x}_{ss} = 0 = (A - BK)x_{ss} + BGr \tag{4.24}$$

Isolating x_{ss} and substituting it into the output equation gives,

$$y_{ss} = Cx_{ss} = -C(A - BK)^{-1}BGr \tag{4.25}$$

Since it is desired that $y_{ss} = r$,

$$r = -C(A - BK)^{-1}BGr \tag{4.26}$$

Finally, rearranging the equation gives G,

$$G = -[C(A - BK)^{-1}B]^{-1} \tag{4.27}$$

The initial simulation test was conducted by solving for K and G after arbitrarily defining the matrices,

$$Q = \begin{bmatrix} 1 & 0 \\ 0 & 1 \end{bmatrix}, \qquad R = [1] \tag{4.28}$$

The simulation was run with a flight manoeuver where the aircraft is stepped from 1.5m to 2.5m as shown below in Figure 41.

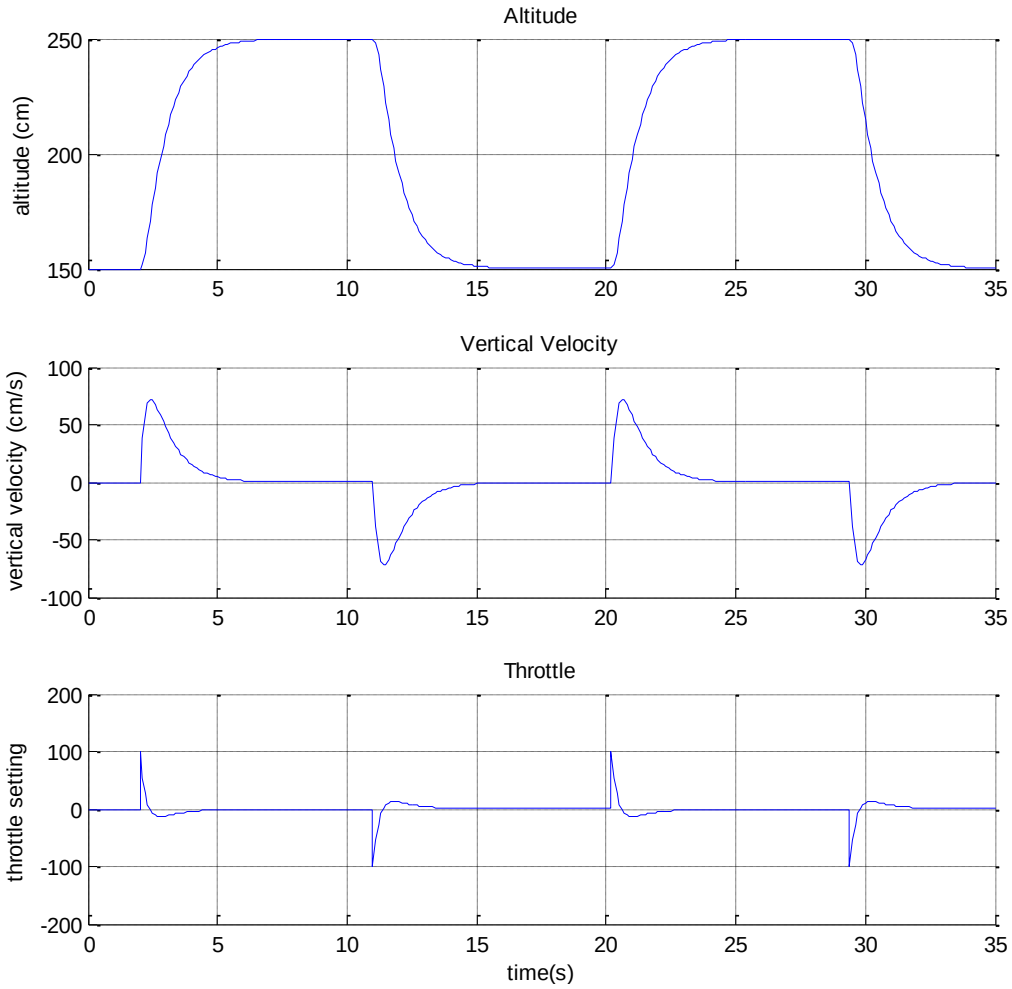

Figure 41: LQR controller test with R = 1

The step response is fast without overshoot which is a reasonable response. Although an issue with this result is the large spike in the throttle during transition indicating the control input might be too high. For safety reasons, the autopilot limits the throttle setting to ± 40. The throttle setting with $R = 1$ greatly exceeds this value. To address this issue the control signal is penalized by setting $R = 5$ before recalculating the controller gains. The result in Figure 42 shows the throttle spike has been significantly reduced and only the tip of the peak passes the 40 mark. This will ultimately lead to a more reliable system because the motor controllers are not being driven as excessively.

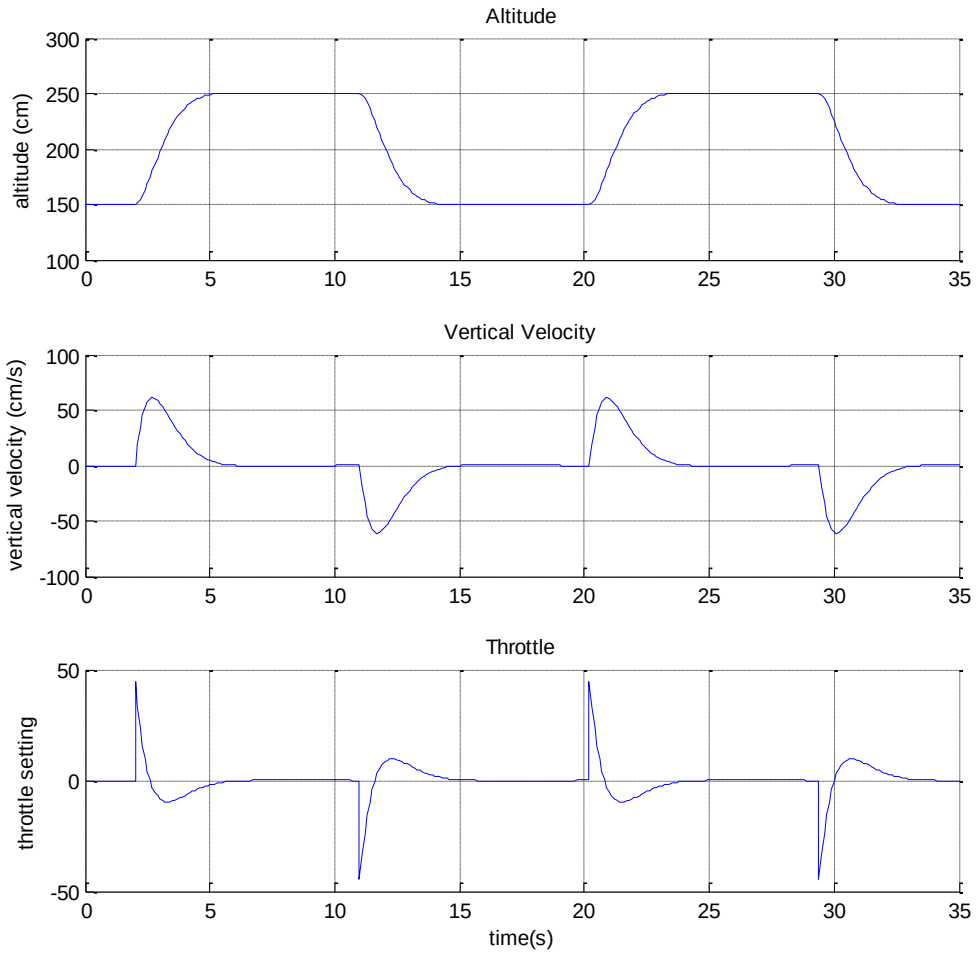

Figure 42: LQR controller test with R = 5

Also interesting is the second set of gains result in a system that has a settling time of 2.9 seconds as opposed to the 3.6 second settling time over the more aggressively driven system.

Chapter 5
Results

In order to evaluate the controller, the Kalman filter and controller were converted into C code for execution in real time within the autopilot. The code was then ported over to the autopilot for in flight testing. Although the design of the Lux is intended only for UAV recovery (ie landing), it is possible to operate the Lux prototype as a VTOL system. As previously mentioned, given the inherently unstable nature of multi-rotor flight, even when the safety pilot has control, the autopilot is required to stabilize the system. Therefore, controller testing on the Lux was executed by first performing an autopilot assisted manual take-off and then the controller was switched on to hold a steady hover. During the flight, the data was recorded to evaluate controller performance.

Initially, some of the requisite data for characterizing the system was gathered while the aircraft was controlled using a PD controller. It became apparent that during a constant throttle hover, the aircraft would drift up and down and was highly susceptible to induced drafts in the room which start after approximately 30 seconds as shown in Figure 43.

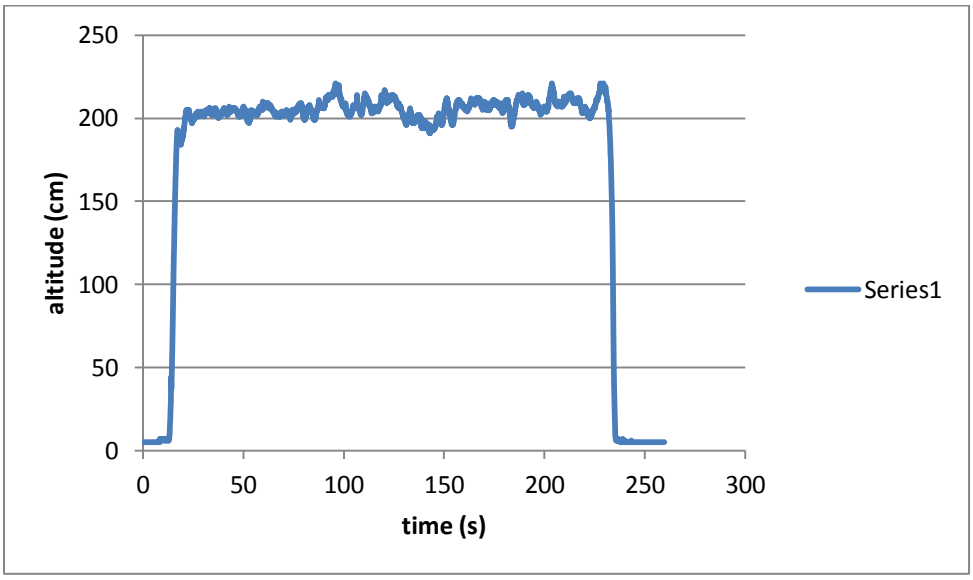

Figure 43: Disturbance effects after 30 seconds of flight due to induced drafts

The drifting was minimized by adding the derivative feedback and the proportional control was included to maintain a set altitude. Since this approach was applied before designing the actual

controller in Simulink, it is beneficial to present the PD results as a baseline to evaluate the LQR controller. The tests were conducted by trying to maintain an altitude of 150cm. Figure 44 shows the result of the PD controller with $P = 0.2$ and $D = 0.1$.

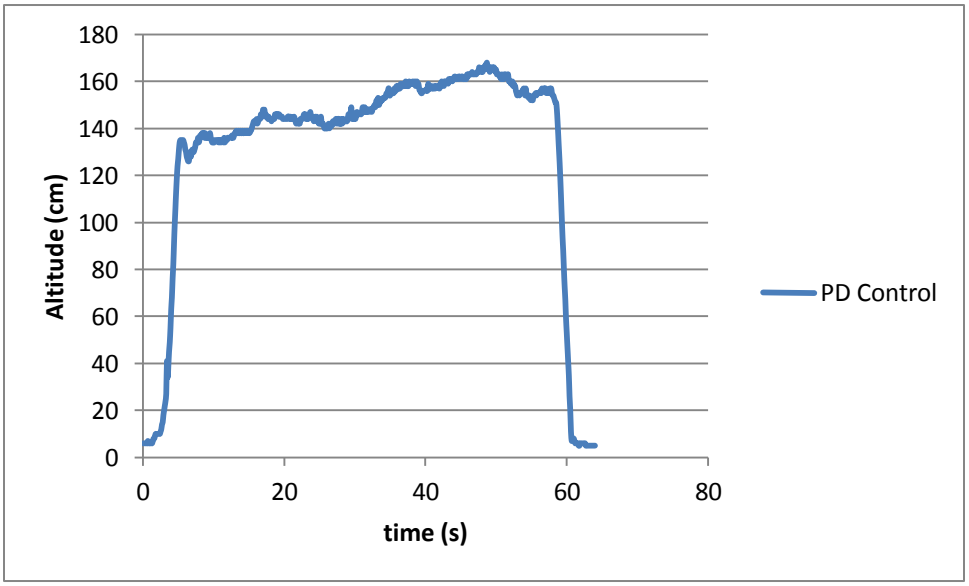

Figure 44: Altitude control using a PD controller set to 150cm (P=0.2 D=0.1)

While the flight appeared to be steady while being conducted, the data shows that the aircraft drifted over the one minute flight. To try to reduce the error while still maintaining the stability, the proportional term was increased to $P = 0.3$ with the results shown in Figure 45.

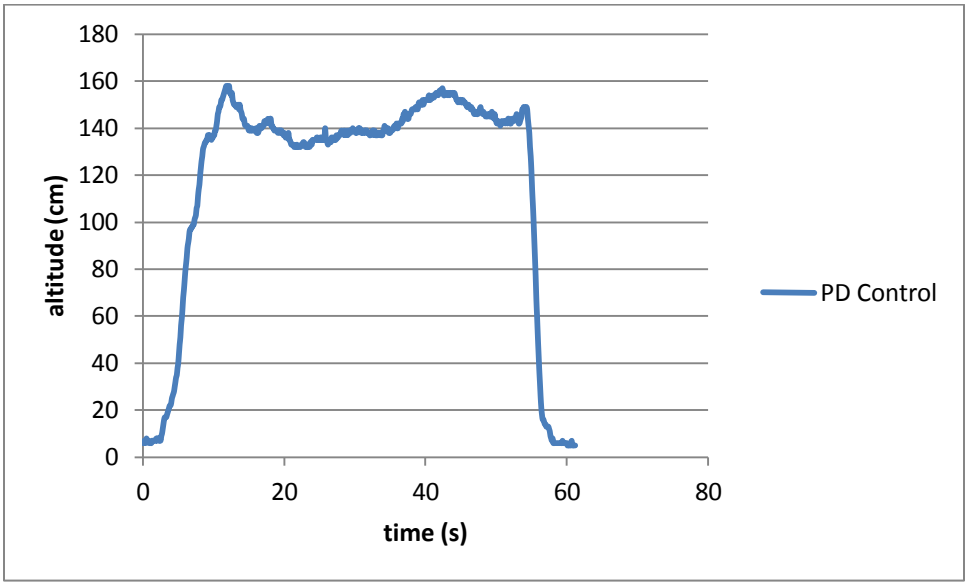

Figure 45: Altitude control using a PD controller set to 150cm (P=0.3 D=0.1)

Once again, the flight appeared steady and the results are indeed better however the data demonstrated a pronounced drift over time. The designed LQR control technique was then tested on the system. Due to uncertainty about how the system would react with the new controller turned on, the gains were recalculated using $R = 20$ to penalize the control input and make the system a little slower than the simulation response. Figure 46 shows the first LQR controller test set to an altitude of 150cm.

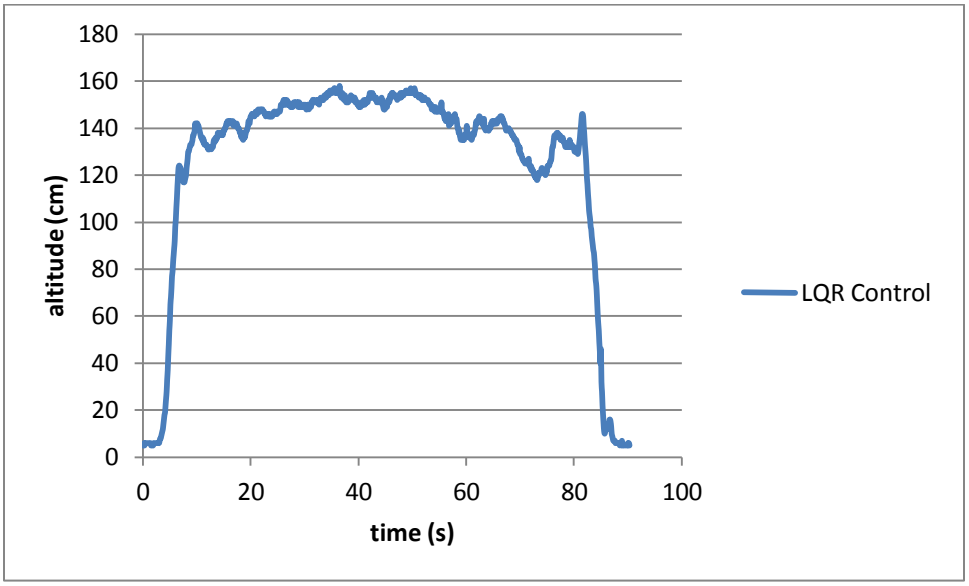

Figure 46: Altitude control using an LQR controller set to 150cm (R = 20)

The controller was stable and functioned as expected with the lower control input. To increase the performance the LQR gains were recalculated with $R = 10$ and the results are shown in Figure 47.

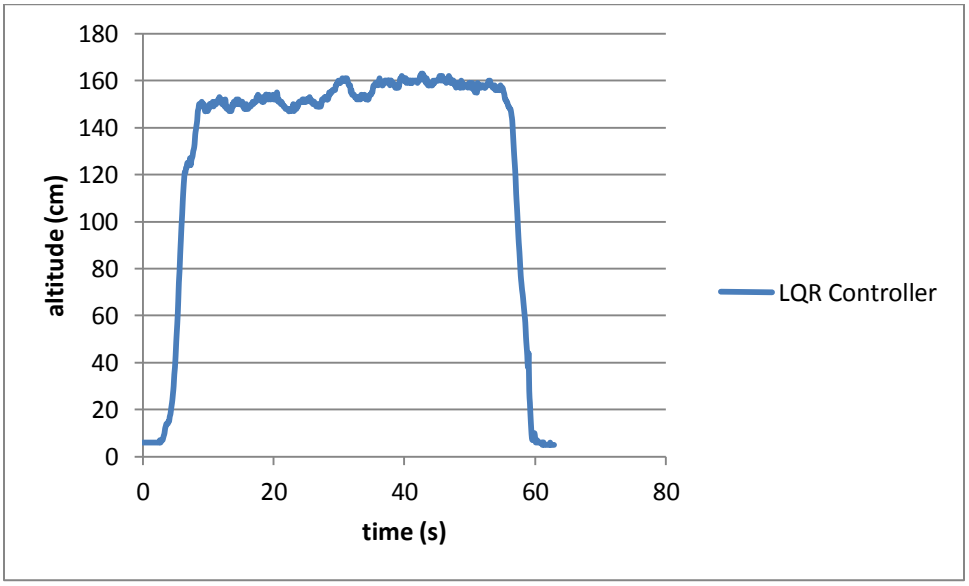

Figure 47: Altitude control using an LQR controller set to 150cm (R = 10)

The LQR controller test is by far the best performance achieved in any of the previous controllers. The test was a minute long flight maintaining an error of less than 10cm which demonstrates the

success of the approach. The PD controllers required much more tuning and still could not achieve this tight control.

Next was to implement the LQR controller that was simulated using $R = 5$. The same step response was applied to the system to compare implemented controller and system to the simulated model shown in Figure 48.

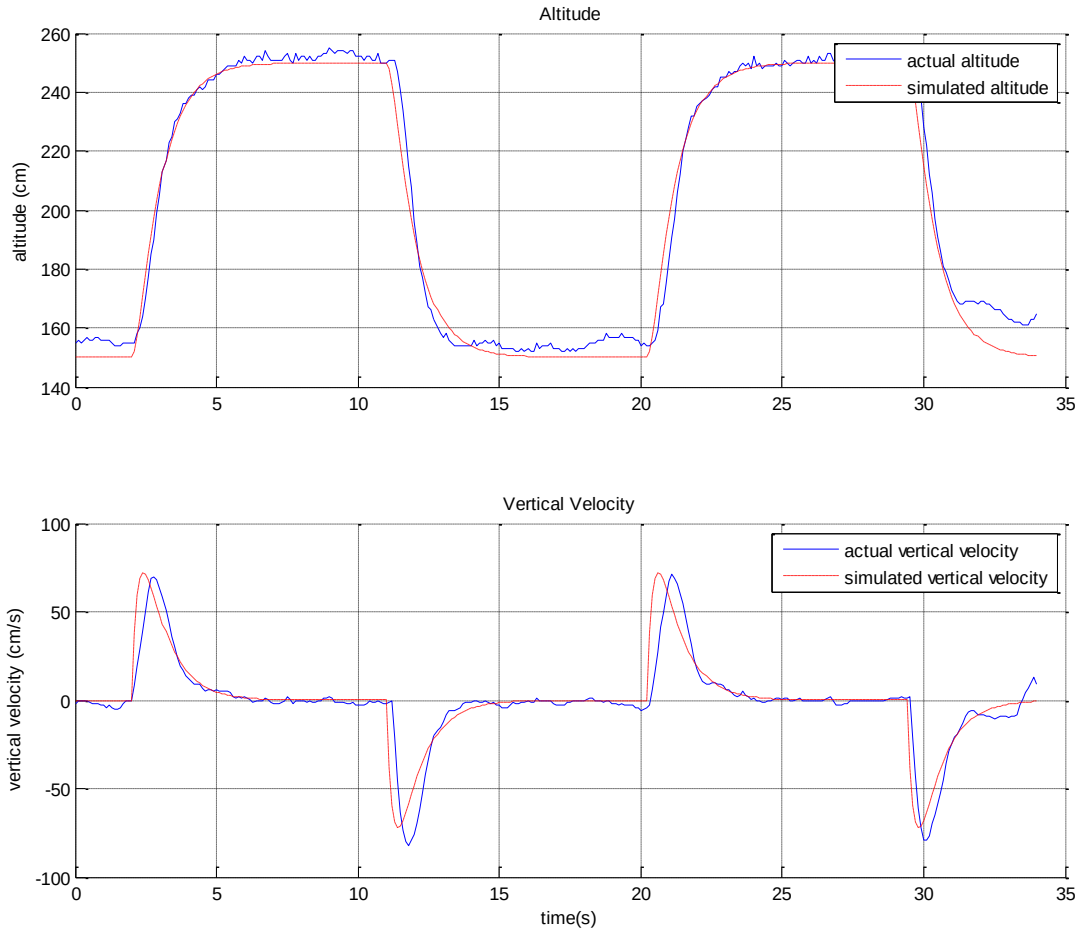

Figure 48: Altitude step control using an LQR controller comparing actual to simulated (R = 5)

The experimental data and simulated response are in close agreement which indicates the identified model is a close fit.

With the altitude control system working, the next step was to evaluate the results by implementing the landing sequence. The key to the autonomous recovery is to use the developed control systems to execute the required manoeuvres to transition from flight altitude to touchdown in a controlled

manner that respects the limitations of the sensors used for altitude control. The main issues that shaped the recovery sequence were:

- The barometric altimeter is the only suitable sensor for altitude control above 3m AGL and it is ideal for relative altitude measurement
- The sonar sensor provides accurate and stable altitude measurements below 3m AGL and is ideal for absolute altitude measurement giving the proper height AGL.
- Altitude control within ground effect is highly non-linear so an alternative control approach would be required

Considering these issues, the recovery sequence was divided into four distinct stages executed sequentially to complete the automated recovery task.

Stage 1 - During the first stage, altitude control is conducted using the barometric altimeter. As was mentioned earlier, this sensor provides high resolution readings that drift over time due to atmospheric conditions. However, its relative accuracy is very good which makes it suitable for the stage 1 constant descent manoeuver. The beginning of this stage is indicated by a command to the autopilot to initiate autonomous descent. The prerequisite for this command is autonomous, non-powered, forward flight with a sustained altitude glide used to bleed-off forward airspeed. The autopilot initiates stage 1 flight when the UAV reaches an airspeed just above that which is associated with a stall. When the stage is initiated, the current pressure altitude is sampled and supplied to the descent controller and used as the current altitude set point. Then, using the pressure altitude measurements a constant decent rate is maintained by linearly decreasing the pressure altitude set point to maintain a constant descent rate.

Stage 2 – The objective of this stage is to decelerate the UAV at a constant rate to prepare for touchdown. As the ultrasonic rangefinder gets near to the ground it starts to receive valid pings indicating the absolute altitude AGL. During this time, the UAV is still in the constant descent of stage 1. However the stage 2 Kalman filter, which uses different measurement noise covariance associated with the sonar, is quickly converging as the sonar data becomes more reliable. At a predefined altitude near the ground, stage 2 is initiated and the altitude control is switched to the sonar measurements while the vertical descent rate is parabolically reduced until the aircraft enters ground effect.

Stage 3 – Once the UAV is within ground effect, there is a sudden and drastic increase in lift. This effect makes the current controllers unable to achieve touchdown. To ensure a graceful touchdown stage 2 ensures the UAVs vertical velocity is nearly zero when it reaches the top of the ground effect. Without this manoeuver, the UAV will bounce of the ground effect leading to difficult control prior to touchdown. Stage 3 begins when the UAV is just in ground effect. Since ground effect is a function of the UAVs distance from the ground, it is simple to control the UAV to touchdown by linearly decreasing the throttle until the craft settles on the ground.

Stage 4 – Finally, immediately at touchdown the throttle is quickly ramped to zero to ensure the lift is dramatically reduced thereby preventing the UAVs tendency to bobble on the ground during motor wind-down. Figure 49 below shows the four stages of the autonomous fixed wing UAV recovery.

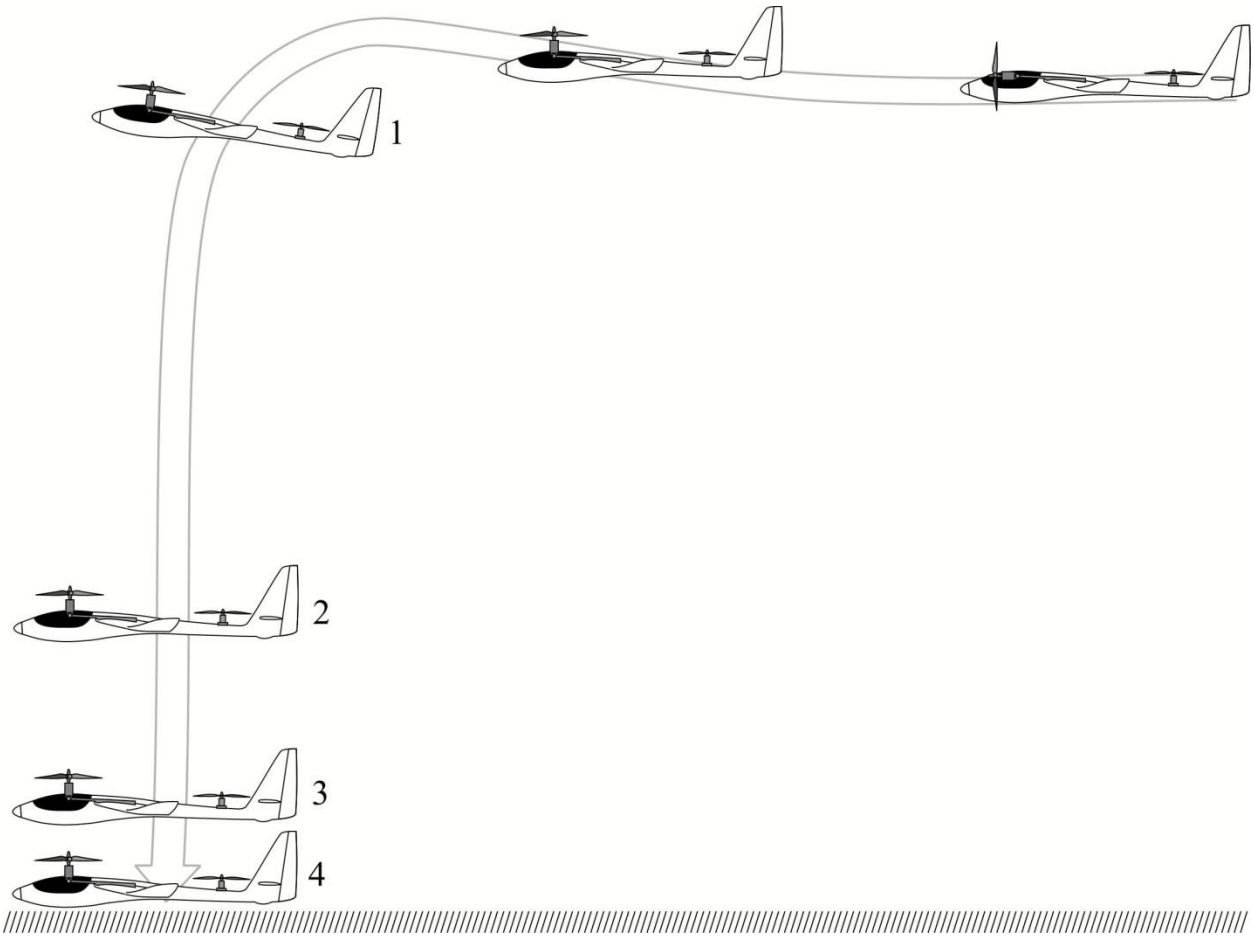

Figure 49: The four stages of autonomous descent, 1 – constant descent using pressure altitude reference, 2 – parabolic deceleration using sonar reference, 3 – descent through ground effect, 4 – motor wind down after touchdown

Using this four stage sequence, a UAV is able to gracefully and easily transition from flight altitude to the ground using the proposed controller and appropriately switching modes of operation. To generate the complete manoeuver in a sequence of four stages, it was necessary to implement a state machine within the autopilot so that transitions from one stage to another are clearly and safely defined. Important when devising such state transitions is the careful consideration necessarily applied to ensure the sequence continues reliably even during abnormal flight conditions. For instance, it was mentioned that stage 1 is started once the airspeed is reduced to just above stall conditions. A safety margin is required to ensure stage 1 execution occurs prior to any type of stall (such as a tip stall) that may occur at higher airspeeds if in the presence of turbulence. Premature

stalling could lead to a condition of uncontrolled flight where the airspeed measuring device (typically a pitot tube) maintains a higher airspeed then that which is required to initiate the descent mode. While this example is somewhat contrived, it illustrates the careful consideration that must be employed when considering autonomous state transitions. In any case, UAV control is designed and required by governing agencies to ensure it is possible for the safety pilot to takeover should autonomous flight run into such issues.

Prior to stage 1 execution presumably the autopilot is controlling the aircraft in forward flight mode and is directing the aircraft on a path into the wind towards the landing site. At the appropriate time the autopilot cuts the throttle and puts the motors into the vertical descent orientation. At this point, the vertical descent mode is armed and triggered once the airspeed requirement is met. A level glide is maintained by the autopilot, increasing angle of attack which necessarily causes the aircraft to slow down. At the appropriate airspeed the vertical descent is triggered. This forward flight control is simply mentioned so the reader understands the process leading up to the autonomous recovery. However, this is not further discussed within this thesis. Through experimentation, it has been determined that the actual airspeed when beginning the descent manoeuver is not critical however at slower speeds the routine is clearly more graceful.

The state transition from stage 1 to stage 2 is largely dependent on the performance of the sonar sensor employed. Given stage 2 requires the use of the ultrasonic rangefinder for the Kalman filter measurement, it is a necessity that the UAV be close enough to the ground to be within the specified range of the sonar. Also, the closer the UAV is to the ground the more reliable the measurements are. Experiments using the Lux which has a 6m range sonar indicated that its sonar measurements were consistent below 3m without erroneous pings received. Above 3m, there were erroneous measurements that ranged from infrequent at 3m to often at 6m. The sonar reading accuracy is highly dependent on numerous factors such as ground surface quality, pitch or roll angle of the aircraft, ambient noise and possibility of nuisance echoes. By maintaining the stage 1 to stage 2 state transition below 3m, it is likely the controller will have the benefit of pristine altitude measurements to ensure reliable control.

The state transition from stage 2 to stage 3 required that it be determined experimentally given that the ground effect in this case is largely due to the shape of the aircraft as well as the position of the propulsion system. Slowing the aircraft prior to reaching ground effect is desirable in order to prevent

the aircraft from bouncing off the ground effect. To characterise the influence exerted on the aircraft due to ground effect, an experiment was conducted by cautiously causing the aircraft to descend towards the ground while graphing the altitude. Figure 50 below shows the UAV's response to the linearly decreasing altitude reference.

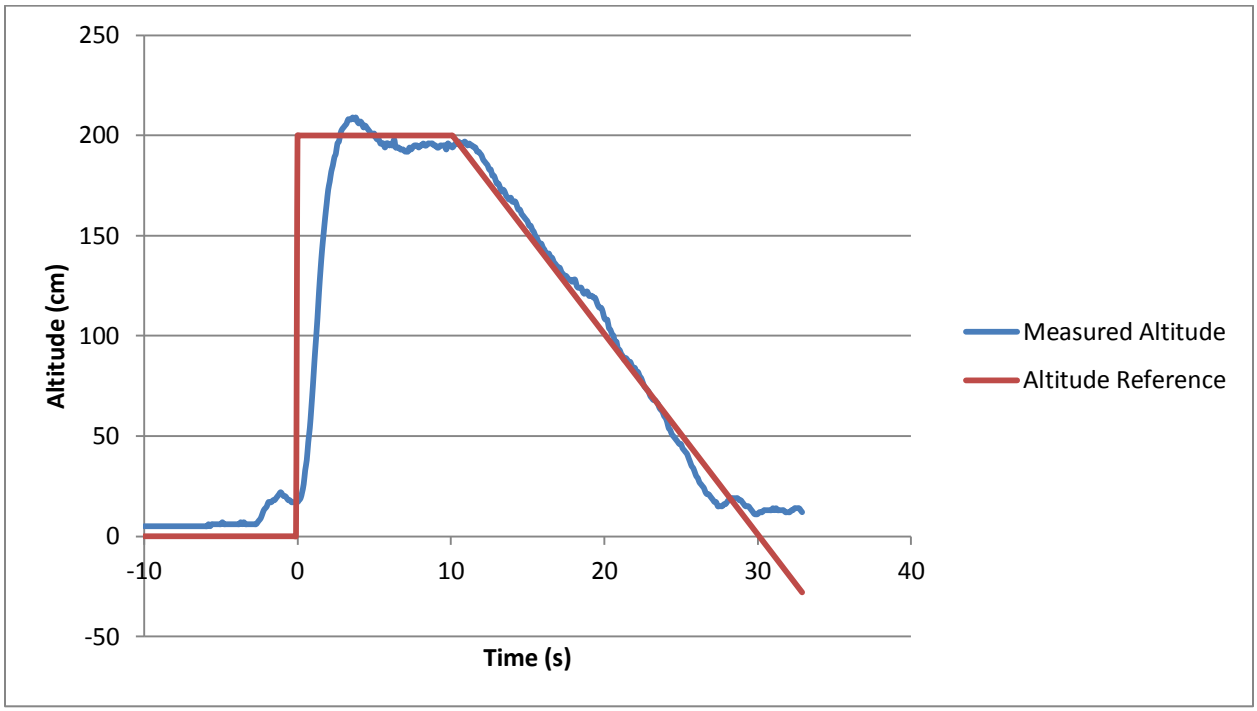

Figure 50: Controlled descent at 10cm/s for investigating ground effect

The controller is enabled at t=0 when the Lux is just idling above the ground and it quickly jumps up to the 2m set point. After ten seconds, the altitude reference is programmed to decrease at a rate of 10cm/s. At approximately 20cm, the ground effect causes the aircraft to bounce back up regardless that the reference altitude applied to the controller continues to decrease. While the experiment was concluded shortly after the aircraft was firmly within the ground effect, tests demonstrated that the altitude error input to the controller had to reach very excessive levels before the aircraft would start to overcome the ground effect. Using the data above, it was determined that the change from stage 2 (descent deceleration) to stage 3 (descent within ground effect) for the Lux should occur at an altitude of 20cm AGL.

Stage 3, the final flying stage of the autonomous recovery, is the descent through the ground effect. The ground effect is most pronounced when operating the aircraft near the ground. The ground

imposes a boundary layer which restricts the downwash shed from the motors thereby increasing the effective lift without changing the RPM of the motors [27]. To descend through this area of increased lift, the throttle is linearly ramped down and the aircraft slowly settles onto the ground. Figure 51 shows the autonomous descent and landing.

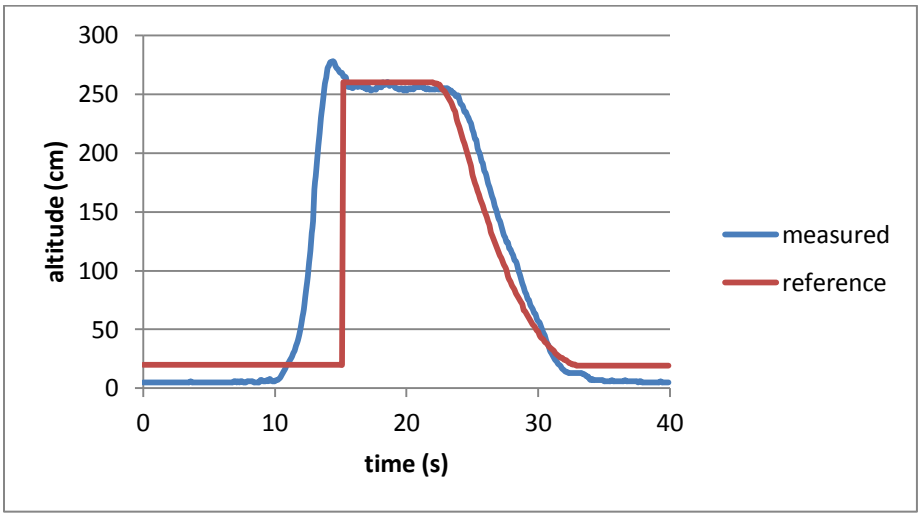

Figure 51: Descent manoeuvre and landing

The Lux was controlled manually to an altitude of about 260cm and then the controller was enabled. After ten seconds, the navigation processor sends the Lux down at 40cm/s and initiates a constant deceleration until the commanded altitude reaches 20cm. Immediately the throttle is ramped down reducing the lift due to the ground effect which allows the Lux to settle onto the ground. This stage is open loop control and the ramp rate determines how quickly the aircraft settles. Due to the nature of open loop control, changes to the aircraft configuration or weight will have an effect on the resulting performance.

Stage 4 occurs once the aircraft is on the ground and is simply a rapid throttle ramp down to turn the motors off. This requirement ensures that a sudden gust of wind or another disturbance does not cause the aircraft to hop back into the air.

The four stages presented here complete the autonomous recovery routine. Repeated indoor tests have shown a gentle descent and touchdown when under autonomous control are able to be executed with precision. The LQR controller, using a Kalman filter state feedback, has been proven to operate reliably and on a consistent basis.

Chapter 6
Conclusions

This thesis explored the issue of autonomous fixed wing UAV recovery with the desire to provide a safer means of concluding UAV missions. Current recovery techniques employed for UAV recovery in developed areas was introduced with a brief discussion of their shortcomings. In order to investigate alternatives, the experimental research airship called the Lux Aether, was introduced and described as an alternative aircraft design employing vertical landing propulsion. A survey of background and parallel research was provided. A short analysis on the experimental system dynamics was undertaken and an approach to decoupled control was provided which allowed a more focus treatment of the altitude associated plant and related control system. While not the focus of this thesis, airframe stabilization was also presented indicating that developing a decoupled system assumption with respect to the longitudinal and lateral dynamics, was reasonable. It was found that PD control of the roll and pitch axis resulted in a stable system ideal for autonomous recovery applications. A number of detail and solution approaches related to trimming the system were introduced as a prerequisite to the system identification and controller design. Because the closed loop control techniques depend greatly on the quality of the sensor readings, different sensor options were explored. Based on both reliability and resolution, the barometric altimeter as well as the ultrasonic rangefinder was recommended as feedback devices.

Various approaches to system identification were explored with varying success. It was identified that using a least squares characterization did not provide accurate results in spite of the methodical approach required to identify the unstable system. Running the system in open loop during the identification process did generate a successful model. Using the system model and sensor variances, a Kalman filter was designed which provided smooth and accurate data regarding system altitude and vertical velocity states. Optimal state feedback control was first perfected in simulation and then implemented within the Lux's autopilot. Using LQR control techniques resulted in a very stable system. The controller was compared with previous PD controller results and it was found that the LQR was by far superior. The success of the LQR control approach validated the system modeling techniques. It was demonstrated that by applying the approach to system identification and using the LQR state feedback controller, the altitude mode could be successfully controlled enabling vertical landing recovery of fixed wing UAV's.

This thesis presents a novel vehicle that can be applied in current commercial UAV applications which provides a built in recovery approach that is safer and more efficient then current fixed wing UAV recovery techniques. This thesis also introduced a successful approach to VTOL modeling techniques that could be generalized to other types of aircraft. Using this developed model, an autonomous landing procedure was introduced that efficiently applies available sensor data to generate a smooth and contiguous landing maneuver. All of the above techniques were validated by testing on an actual aircraft system.

6.1 Future Research

For the specific stages of UAV recovery, the topic of this thesis, further investigation into optimizing the recovery process for efficiency is an area where more investigation is required. Namely, problematic was that when a mission was completed, the amount power left in the battery was minimal due to current autonomous descent which demands a lot of power. While the focus of this thesis was placed squarely on the control aspect of the recovery, the aircraft used was designed to sustain lift for data gathering experiments and was generally overbuilt. Future revisions would look at decreasing the size of the motors to better match the minimum requirements while optimizing the propeller for both forward flight and vertical descent phases. Using this more optimized platform and leveraging the control system explored in this thesis, more advanced descent manoeuvres could possibly be explored. Ideally, this vertical UAV recovery system could use smaller motors that simply stabilize the aircraft in a gravity powered descent and decelerate the craft prior to touch down. This type of experimentation requires a solid control foundation to build upon since the experiments would require hand launched flight to achieve altitude before the descent tests could be evaluated. Once the descent is initiated, the aircraft is committed to the manoeuvre so there is a smaller margin of error to ensure the aircraft is not lost to a crash.

Other future research could include investigating the transition from forward flight to vertical descent under autopilot control. The stability and control of fixed wing aircraft flight dynamics are well understood. The equations are based on aerodynamic derivatives which influence the system according to states of the system such as angle of attack and sideslip. These techniques are heavily based on the velocity and orientation of the wind frame with respect to the body frame. At the very low airspeeds encountered when transitioning to descent mode these equations start to break down since the derivatives are generated by linearizing the system about an operating point. To robustly operate a control scheme from forward flight to vertical descent, a unique topology would have to be explored to handle the transition.

The research in this thesis has demonstrated a model structure with proven accurate control results. Further research into the suitability of adaptive control would be beneficial. Using adaptive control techniques, changes in the aircraft structure or payload would be accounted for without having to redo the system identification. Leveraging the developed model, adaptive control techniques could be applied for the model parameter identification. Future research would extend the capabilities of the

system. Further research could lead to online parameter identification or an offline method used for autonomous tuning of the system.

The Lux Aether UAV has extended the possible applications of efficient fixed wing UAVs. Anywhere a helicopter or multi-rotor UAV can operate is now an ideal location to conduct fixed wing UAV missions. In northern areas, where the landscape is either forested or covered by undulating rocks, missions can now be conducted out of a small clearing. Longer range fixed wing operations such as dropping GPS transponders on icebergs can now be conducted on the oceans using vessels that are not designed for fixed wing aircraft recovery. Finally, a major benefit of the system is the autonomy. The most difficult part of flying conventional aircraft is the landing, by automating the landing procedure, the UAV applications can extend to those which do not require qualified pilots.

References

[1] M. Degarmo and G. Nelson, "Prospective Unmanned Aerial Vehicle Operations in the Future National Airspace System," in *AIAA 4th Aviation Technology, Integration and Operations (ATIO) Forum*, Chicago, Illinois, Sep. 20-22, 2004.

[2] (March, 2013) Accuas. [Online]. http://www.accuas.com

[3] (2013, March) Unmanned Systems Canada - Student UAV Competition. [Online]. Internet: http://www.unmannedsystems.ca/content.php?sec=8

[4] P. G. Fahlstrom and T. J. Gleason, *Introduction to UAV Systems*, 4th ed., John Wiley & Sons Ltd, Ed. Chichester, UK: John Wiley & Sons Ltd, 2012.

[5] J. Rumerman. (2010, December) Early helicopter technology.

[6] J. G. Leishman. (2000) The history of helicopter flight. [Online]. http://terpconnect.umd.edu/~leishman/Aero/history.html

[7] J. G. Leishman, *Principles of helicopter aerodynamics*. New York, NY: Cambridge University Press, 2000.

[8] O. Stewart, "New ways of flying: the Trueman Wood lecture," *Journal of the Royal Society of Arts*, pp. 626-640, May 1955.

[9] D. L. Kohlman, *Introduction to V/STOL airplanes*. Ames, IA: Iowa State University Press, 1981.

[10] T. McLelland, *Harrier*. Birmingham, UK: Ian Allan Publishing, 2011.

[11] Julian. (2013, March) Harrier and F-35B. [Online]. http://juliantheaviator.wordpress.com/2008/01/15/harrier-and-f-35/

[12] V. Fuertes, A. Piquereau, R. Mampey, and F. Teichteil-Königsbuch P. Fabiani, "Autonomous flight and navigation of VTOL UAVs: from autonomy demonstrations to out-of-sight flights," *Aerospace Science and Technology*, vol. 11, no. 2, pp. 183-193, 2007.

[13] J. H. Lee, B. J. Kim,H. J. Kwon,E. T. Kim, A. Iee-Ki P. S. Kim, "Automatic Landing Control Law for Unmanned Helicopter using Lyapunov Approach," *25th Digital Avionics Systems Conference*, vol. 1, no. 8, pp. 15-19, October 2006.

[14] C. Ham, Z. Qu, J. Kaloust, "Nonlinear autopilot control design for a 2-DOF helicopter model," *Control Theory and Applications, IEEE Proceedings*, vol. 144, no. 6, pp. 612-616, November 1997.

[15] J. F. Montgomery, G. Sukhatme, S. Saripalli, "Vision-based autonomous landing of an unmanned aerial vehicle," *IEEE International Conference on Robotics and Automation, Proceedings*, vol. 3, pp. 2799 - 2804 , 2002.

[16] J. Stumpf, M. Achtelik, K. M. Doth, G. Hirzinger, D. Rus D. Gurdan, "Energy-efficient Autonomous Four-rotor Flying Robot Controlled at 1 kHz," in *2007 IEEE International Conference on Robotics and Automation*, April 2007, pp. 361-366.

[17] R. Siegwart S. Bouabdallah, "Backstepping and Sliding-mode Techniques Applied to an Indoor Micro Quadrotor,"" in *Proceedings of the 2005 IEEE International Conference on Robotics and Automation*, 2005, pp. 2247-2252.

[18] E. Altug B. Erginer, "Modeling and PD Control of a Quadrotor VTOL Vehicle," in *2007 IEEE Intelligent Vehicles Symposium*, 2007, pp. 894-899.

[19] (2012, March) CropCam images on demand. [Online]. http://www.cropcam.com

[20] G. M. Y. Lai, "Modelling and control of small-scale helicopter on a test platform," *Doctoral Thesis - University of Waterloo*, 2008.

[21] Q. G. Wang, *Decoupling Control*. Berlin, Germany: Springer, 2003.

[22] B. Etkin, *Dynamics of Atmospheric Flight*. New York: John Wiley & Sons, 1972.

[23] R. W. Beard and T. W. McLain, *Small Unmanned Aircraft Theory and Practice*. Princeton, NJ: Princeton University Press, 2012.

[24] R. C. Nelson, *Flight Stability and Automatic Control*, 2nd ed. Boston, MA: McGraw-Hill, 1998.

[25] G. Welch and G. Bishop, "An Introduction to the Kalman Filter," *In Practice*, vol. 7, no. 1, pp. 1-16, July 2006.

[26] R. C. Dorf and R. H. Bishop, *Modern Control Systems*, 11th ed. Upper Saddle River, NJ: Pearson Prentice Hall, 2008.

[27] B. Etkin and L. D. Reid, *Dynamics of Flight stability and control*. Danvers, MA: John Wiley and Sons, 1996.